POLITECNICO DI TORINO

Master of Science in Aerospace Engineering

MASTER'S DEGREE THESIS

Analysis of innovative aerodynamic devices on production vehicles

Supervisor:
ARINA Renzo

Co-Supervisor:
CORRE Christophe

Company Supervisor:
GORAGUER Yann

Candidate:
CEMBALO Agostino

ACADEMIC YEAR 2020-2021
April 2021

Abstract

Yaw angles in a car's real environment are for 80% of the time different from zero, as has been proven by [1] and [2]. The reduction of car emissions is one of the significant challenges among automotive companies, including the PSA Group. Hence, the interest in studying solutions that can adapt to the environment around the vehicle increases. Our work shows the interest in having mobile aerodynamic devices concerning the vehicle's speed/yaw condition. We observe a drag reduction of around 1%, which is remarkable on a vehicle's scale. Besides, we would also like to build a database to prepare a doctoral thesis, in which, eventually, we will be able to implement the identified solutions on a production vehicle. We designed CAD parts and we tested them in a wind tunnel on a reduced scale during this study, more precisely on ¼, at the GIE-S2A in Montigny-le-Bretonneux. The interest of having mobile aerodynamic devices on the rear window of the vehicle is proven, which brings a significant improvement of the pressure field at the base and improves the associated drag. Post-processing of the data shows promising results. The vehicle's drag is significantly improved, while its lift has only a slight degradation. We observe negligible differences in the yawing moment of the car. Configurations with symmetrical flaps are not necessarily always beneficial. We identified configurations with two asymmetrical flaps that have better performances.

Acknowledgements

Even though its relatively short length characterizes this work, it results from a journey that began in 2012. All along this journey, I have been able to confirm, and even increase, my passions for the automotive world. For this, I consider it very important to thank certain people.

I want to thank the PSA Group for allowing me to do a six-month internship, starting from June 2020 until December 2020, in an environment that I have been passionate about since I was very young. This work allowed me to grow both from a personal and a professional point of view. I was able to put into practice what I studied from a theoretical perspective.

A special thank goes to Renzo Arina, who has always been there to help me in case of need. Since the beginning of this incredible experience, he follows me and, eventually, he also agreed to be my academic tutor on the Politecnico's side. Once more, he collaborated to make me the person I'm today.

I want to thank my academic tutor Christophe Corre, who was also my tutor for the second-year internship. He actively participated in my training as a teacher and as a tutor. Without him, I would not be the person I am today.

I would also like to thank Vincent Herbert, head of the SFTA service, who integrated me into his department.

A thank also goes to Guillaume Bonnavion, who was my second company tutor. He was an important figure for me throughout my internship. If I had a question, he was always there to answer, and he gave me incredible support either from work or moral point of view.

I need to thank Yann Goraguer, my company tutor, who has given me a great deal of confidence from the start, and, despite the health context, he has given me the means to carry out a very high-level internship. Throughout this experience, he gave me essential practical and theoretical advice. His skills as an experimenter contributed to add value to this work and allowed me to grow a lot from a personal and professional perspective.

Finally, but not in order of importance, I would like to thank all my family. They have allowed me to be here, but at the same time, I have always felt close to them, even from 2000 km away. Besides, I would like to thank Annalisa, she has been with me for eight years, and there are no challenging moments since I'm with her. Knowing that you are there, next to me, allow me to pass all the challenges without hesitation.

Table of contents

Glossary

<table>
<tr><th>Acronyms - Initials</th><th>Significance</th></tr>
<tr><td>Vehicle Nomenclature</td><td>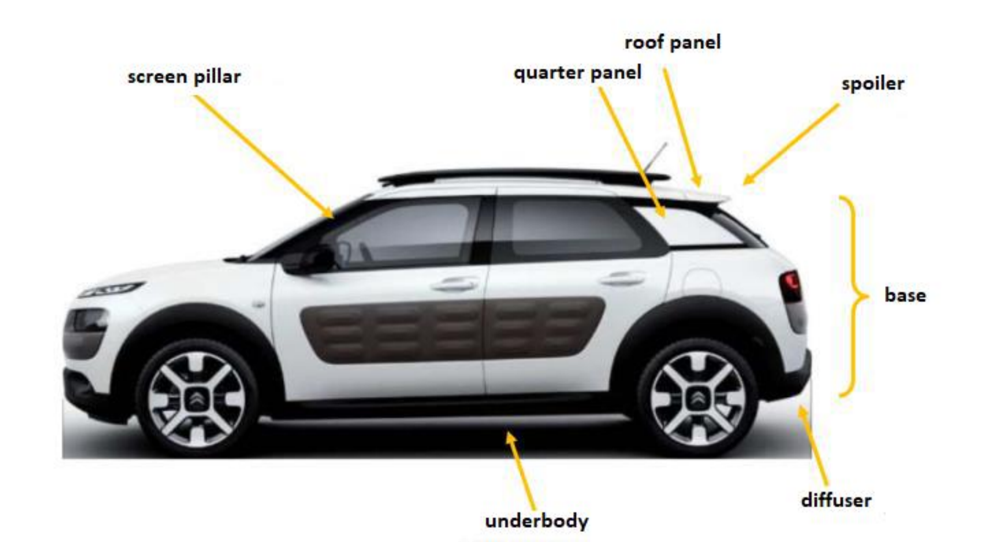
</td></tr>
<tr><td>ABS-M30</td><td>3D printing material that offers good resistance to impact and bending.</td></tr>
<tr><td>CAD</td><td>Computer-Aided Design, we refer to the set of software and geometric modeling techniques that allow to design with the help of a computer.</td></tr>
<tr><td>Flaps</td><td>Spoilers that extend the two rear quarter panels, or side windows, of the rear cab.
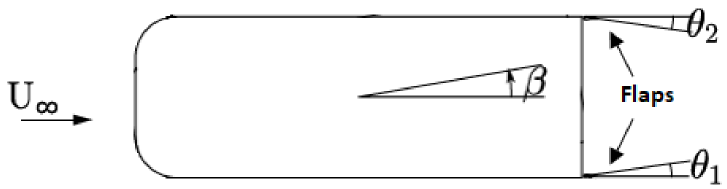

β is the yaw angle of the vehicle. θ_1 and θ_2 are the angles of inclination of the flaps. They are positive if the flaps are tilted towards the rear window and negative if the flaps are tilted outwards.
</td></tr>
<tr><td>DRIA</td><td>Direction for Research and InnovAtion, Research Department of the PSA Group.</td></tr>
<tr><td>Stake</td><td>Result of a comparison between the studied configuration and a reference configuration. For the SC_x the stake is calculated as follows:
ΔSC_x [dm²] = ($SC_{x\,config}$ – SC_{xref}) * 100.
For the Cp, we calculate $\Delta C_p = (C_p - C_{pref})$.</td></tr>
</table>

LAB	Machinable board in epoxy resin or polyurethane with a density ranging from 100 to 1700 $\frac{Kg}{m^3}$.
NEDC	*New European Driving Cycle*, an old vehicle certification test standard, dated 1973, which measures fuel consumption, CO_2 and pollutant emissions.
RDE	*Real Driving Emissions*, test consisting of a very precise path on open roads, included in the WLTP test standard, which allows to have CO_2 and pollutant emission values very close to the real driving ones.
SD2T	*Scientific Department & Disruptive Technologies*, Department of PSA Group.
SFTA	*Science of Fluids, Thermal- and Aeroacoustics*, Department of PSA Group.
WLTP	*Worldwide harmonized Light vehicles Test Procedure*, new vehicle approval test standard, dated 2017, which measures fuel consumption, electric range and CO_2 and pollutant emissions. This standard includes the RDE test.

1. Introduction

In order to complete my academic career, I had the opportunity to join the PSA Group's *Direction for Research and InnovAtion* (DRIA), and more precisely, the *Science of Fluids, Thermal and Aeroacoustics* Department (SFTA), for a 6-month end-of-study project (Master Thesis).

Despite the problematic health context, because of the Covid-19, I had the chance to tackle several subjects throughout my training course, all linked by a common thread, which is emissions in real driving conditions.

If we talk about current matters, we will indeed mention a central theme: global warming. In this context, while working in an automotive company, you are strongly affected by greenhouse gas emissions. We estimate the total number of cars globally at more than 1 billion; understandably, the world's car fleet cannot neglect this aspect. Therefore, all car companies must commit to producing vehicles that are more respectful of nature.

In recent years, the European Commission has made the protection of air quality, and respect for nature, a priority [3]. They aim to encourage this change with incentives. However, to have an absolute rigour, limits have been imposed in terms of polluting emissions and CO_2 grams/Km reduction, which are accompanied by more precise and reliable testing procedures, and, simultaneously, closer to the actual driving conditions. The old test, called NEDC (New European Driving Cycle), which dates to 1973, has only one test on a chassis dynamometer (shown in Figure 1-1). Moreover, being quite old, it was not representative of today's real driving conditions, with many constant speed stages and relatively slow accelerations.

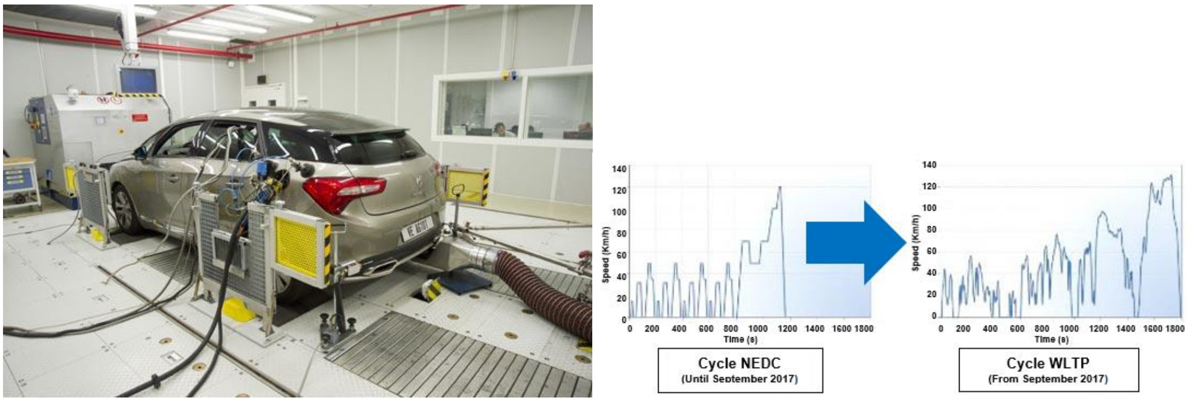

Figure 1-1: On the left-hand side it is possible to see an example of a car on a chassis dynamometer during a test; on the right-hand side it is shown the evolution of the test cycles ([4] and [5]).

From 1 September 2017, the European Commission has imposed new test conditions, all included in the new cycle called WLTP (Worldwide harmonized Light vehicles Test Procedure) shown on the right-hand side of Figure 1-1. This test can reproduce a more usual driving style with more realistic transients. In addition to the chassis dynamometer test, the WLTP is complemented by an RDE (Real Driving Emissions) test, which is the real added value of the WLTP. The RDE test is an open road test that includes three parts: an urban part, an extra-urban part, and a final part on the highway. These three parts are subdivided in a precise way to have a path that can represent as much as possible a real driving condition [6]. During this test, we equip the vehicle under test with an on-board measurement system, shown in Figure 1-2.

Figure 1-2: On-board system in an RDE test [7].

With this on-board system, gas emissions can be measured and compared with the chassis dynamometer test results. Usually, the results are different; the experts already considered this aspect when they introduced the RDE test. That's why they introduced an overrun coefficient for each measured element. The presence of this coefficient is explained because we don't consider many things during the chassis dynamometer test, such as the wind's effect, the variation of the car's attitude, the road conditions, the driving environment, the change of wheel direction, etc. Besides, there are flow conditions that vary from those observed in the wind tunnel. There is a turbulence rate due to the atmospheric layer. Also, there are controlled conditions during wind tunnel tests and often a zero-yaw angle (Figure 1-3). In contrast, road conditions are different and therefore drag values are higher because of the yaw angle, which has been shown by previous internal studies, as well as by academic researchers' studies ([8], [2], [1], [9]).

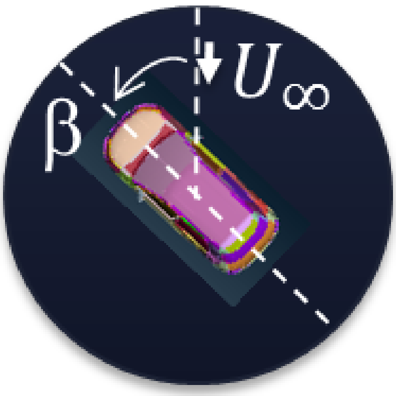

Figure 1-3: Definition and convention of the yaw angle

I was lucky. During the internship, we were able to work on several subjects, which plunged me directly into the work of the everyday engineer and allowed me to progress a lot. The challenge for the PSA Group is to reduce consumption and pollutant emissions. In this context, we had the opportunity to study, experimentally, the influence of the yaw angle on a vehicle, trying to use specific devices to always have an optimum configuration that guarantees minimum drag. This last point is also preparatory work for a doctoral thesis on adaptive aerodynamics.

This master thesis is a summary of the work carried out within the PSA Group throughout my internship. I will first briefly introduce the Group. Secondly, I will present the bibliography related to the traineeship's subject to show the studies' state of progress. Also, I wrote two additional chapters: one to detail the rear cabin's design phase and the other to present the wind tunnel test results. Finally, I wrote a final chapter, including the conclusions and the personal point of view.

2. Presentation of the working context

Unfortunately, my internship took place at a time of global health crisis, the Covid-19 related health crisis. For this reason, I started my internship with the first half-day in the company to have access to the tools necessary to work from home and most of the following days in smart-working.

The internship was supposed to start at the end of March 2020, but because of the sanitary context, we needed to postpone it to the end of June 2020. This rescheduling allowed me to take advantage of a certain number of sessions in the wind tunnel as well as days of instrumentation and handling of specific tools. The PSA Group has always been very attentive to its employees and collaborators. Quite strict protocols have been adopted, which has enabled us to do our work safely.

Hereafter, we will first present the PSA Group and then the GIE-S2A wind tunnel in which we could carry out the programmed tests.

2.1. Presentation of the PSA Group

As a world-class French automotive company, which has been helping to write the automotive world's history for a very long time, the PSA Group does not need a presentation. At the same time, it is good to describe the context I was part of for six months.

The PSA Group, which includes the automobile brands Citroën, DS Automobiles, Peugeot, as well as Opel, Vauxhall, and the mobility operator Free2Move, is organized around a Supervisory Board (SB) and a Management Board (MB). The latter provides executive management. It also contributes to the definition and implementation of strategy, following the Supervisory Board's main guidelines. The Management Board is appointed for four years by the Supervisory Board and comprises four members, including a Chairman. A diagram of the current Board of Directors is shown in Figure 2-1 below.

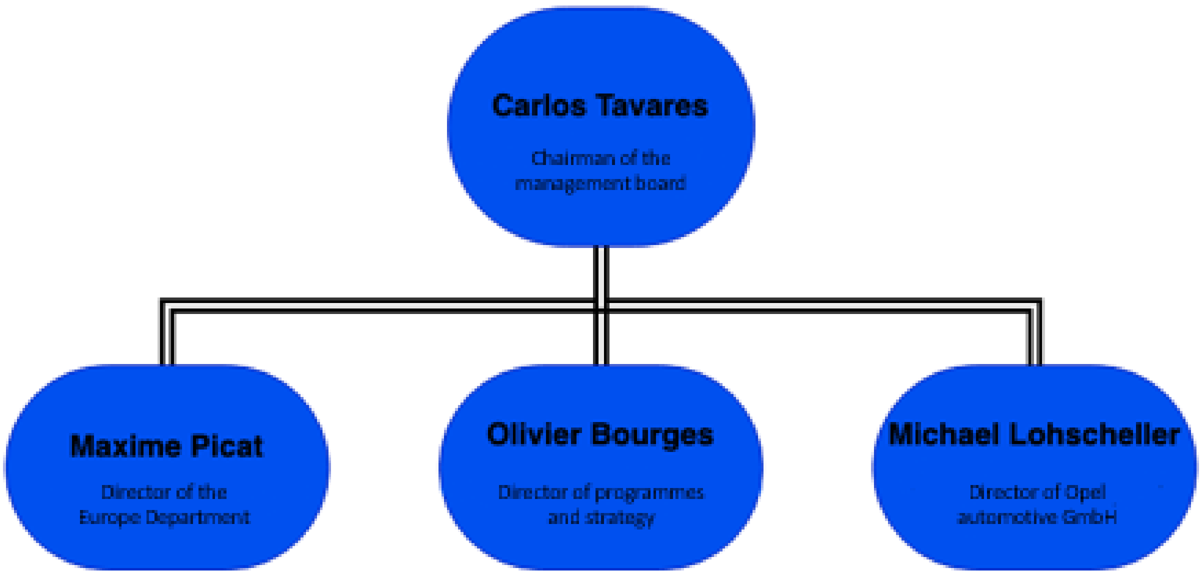

Figure 2-1: Organisation chart of the PSA Group Management Board.

The Supervisory Board ensures permanent supervision of the management of the Company by the Management Board. It defines the major long-term guidelines for the actions of the Management Board. The General Meeting of Shareholders, of which the current Chairman is Mr. Louis Gallois, appoints the Management Board for a four-year term.

Within this framework, we can find the *Direction for Research and InnovAtion* (DRIA), headed by Mrs. Carla Gohin, and the *Scientific Department & Disruptive Technologies* (SD2T), led by Mr. Ladimir Prince. The latter includes the *Science of Fluids, Thermal and Aeroacoustics* (SFTA) department, of which I was a member for this brief period.

Innovation for the PSA Group revolves around customers by following a triptych of innovation. The objectives are several, and we can group them as follows:

- Innovate to meet customer expectations
- Innovate to limit the impact on the environment
- Innovate to offer more attractive automotive products.

Therefore, it is essential, for every idea, to respect these three points, without which it would not be possible to meet either the requirements and tastes of customers or the strict standards imposed by the European Commission.

On the scientific level, at PSA, each idea is associated with a scale that establishes the maturity of the innovation itself. This scale is called *Technology Readiness Level* (TRL) and is based on nine levels.

At PSA, TRLs 1 to 3 corresponds to the beginning of innovation, i.e. the moment when someone has an idea and tries to develop it. TRLs 4 to 6 correspond to the industrialization phase. Thus, the DRIA deals with TRLs 1 to 6, from the creation to the industrialization of an innovation. Other departments then take over for the application and development of the design, up to TRL 9, where the innovation is finally embedded on the vehicle. Figure 2-2 shows the definition of the TRL scale for the PSA Group.

TRL	Objectives and Milestones
1	If we have an idea that we think we have potential to become an innovation then we fill out an "Idea Sheet". This sheet aims to be replivated to be used when one will work on a similar subject in innovation. It is also used to not work twice on the same subject. A jury report grants or not the passage of the milestone called JOS.
2	At this stage a validation of the concept on a Small scale model or by numerical simulation is needed. A DSM (Scientific Maturity report) must be written and validated during a meeting with both quality and innovation managers of the innovation department. This meeting is a milestone called JIS.
3	The concept must be tested on a full scale model. Results are presented and validated (or not) by the same jury as for TRL2 (JIS). This milestone is called JOT and reaching it means that the concept is taken by the innovation department ACBI (Advanced, Chassis Body and Interior).
4	ACBI works on the reliability of the concept and the impact that it could have on other domains (thermal, acoustics, design...) or parts of the vehicle. ACBI also evaluate the cost of the innovation and the potential difficulties of in case of a large scale industrialization. This department is competent in all domains in interaction with aerodynamics (frame, bodywork, ground linking) but have no expertise in aerodynamics. A strong interaction with the scientific department (SFTA - TRL 1 to 3) and the project department (ARO – TRL 7 to 9) is then necessary
5	
6	
7	The innovation is transmitted to the project aerodynamics department (ARO). Their work is to include the innovation in a new vehicle project and then reach TRL 9. This milestone is called ECVR.
8	
9	

Figure 2-2: TRL scale of PSA Group.

2.2. Presentation of the GIE S2A wind tunnel

Three organizations finance the *Groupement d'Intérêt Economique Souffleries Aéroacoustiques Automobiles* (GIE S2A) under a common agreement, i.e., the PSA Group, Renault, and the Conservatoire National des Arts et Métiers (CNAM). This *Groupement* has been operational since 2003 and offers two wind tunnels whose performances place them among the best in the world. These performances are updated every year, and we can also use acoustic modules and Particle Image Velocimetry (PIV) techniques, which allow fascinating flow analysis.

The two wind tunnels are different in size and test characteristics; S2A allows full-scale and reduced-scale testing. Personally, up to now, I have had the opportunity to assist and to pilot reduced-scale tests, so below, we will detail only this one. A detailed presentation was made by [10] and [11].

The reduced-scale wind tunnel offers several possibilities, including tests with boundary layer suction and tests with variable yaw angles.

Figure 2-3 shows a simplified diagram of the complete aeraulic circuit.

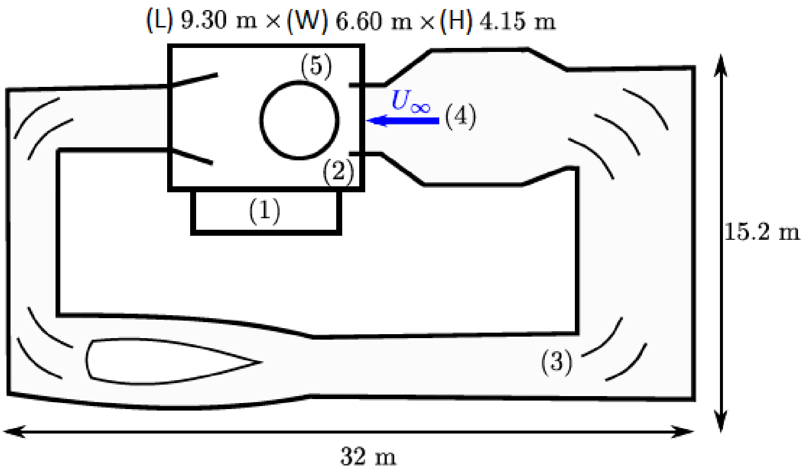

Figure 2-3: Simplified diagram of the complete aeraulic circuit of the reduced-scale wind tunnel with its characteristic dimensions [11].

This wind tunnel's overall footprint is 32 m x 15.2 m. The plenum's size is of 9.30 m in length, 6.60 m in width, and 4.15 m in height. The vein is of the type ¾ open, which is justified by the presence of a plenum (2). The maximum speed of the flow is 240 km/h. We can see four 90° bends, which direct the flow towards the convergent before entering the plenum. The number of straighteners in the turns is not uniform, but this is specifically intended to have the most uniform flow possible. Three grids minimise the flow turbulence; there is also space for a honeycomb flow straightener, which it is not mounted. All this means that the turbulence rate and the flow's non-uniformity at 160 km/h is less than 0.5%.

In the reduced-scale wind tunnel, two boundary layer hoovers control its thickness to not influence the flow around the vehicle. The floor under the car is fixed, so unlike in the full-scale wind tunnel, it is impossible to simulate the moving ground. The non-rolling ground has a significant influence on the results. However, the purpose of the reduced-scale tests is to check innovations in a first approach. Since the floor does not scroll, the tests are cheaper than the full-scale wind tunnel. However, we must be aware that if the tested ideas are valid, they will have to be developed for a full-scale wind tunnel session that gives us a more complete and realistic measurement.

The rotating table (5), with a diameter of 2.1 m, allows a rotation of -30/+30° with an accuracy of ±0.1°. There is a 3-axis/6-component balance system and four masts on which we place the model that we want to test. This system allows the measurement of forces and moments, from which we have the SCx, SCy, SCz, SCl, SCm, and SCn with an accuracy of 0.1 dm^2.

Figure 2-4: Top-left 3-axis, 6-component balance seen from below; Top-right blower motor-fan of the reduced-scale wind tunnel; Bottom-left flow straighteners placed in one of the four corners of the wind tunnel; Bottom-right Plenum of the wind tunnel seen from the convergent.

The full-scale wind tunnel is more complete, but each session's cost is about 4.5 times higher. For this reason, the reduced-scale wind tunnel is much more used by our department. The innovations tested in the full-scale are those that gave satisfactory results in the reduced-scale tests.

3. Preparatory bibliographical study

This chapter shows the bibliographical research inherent to the work carried out during my internship since it is crucial to understand the starting point of our studies.

We will analyse the behaviour of the car's wakes as a function of the yaw angle. Since the drag produced in the car's wake is significant, compared to the other sources, it is important to understand the wake's physics. This aspect allows us to know how to act positively in terms of drag and emissions reduction by analysing the correlation between incident flow and base pressure.

3.1. Incident-flow/base-pressure correlation

Each car manufacturer aims to design a car that is as optimised as possible while respecting the various constraints in order to maximise sales.

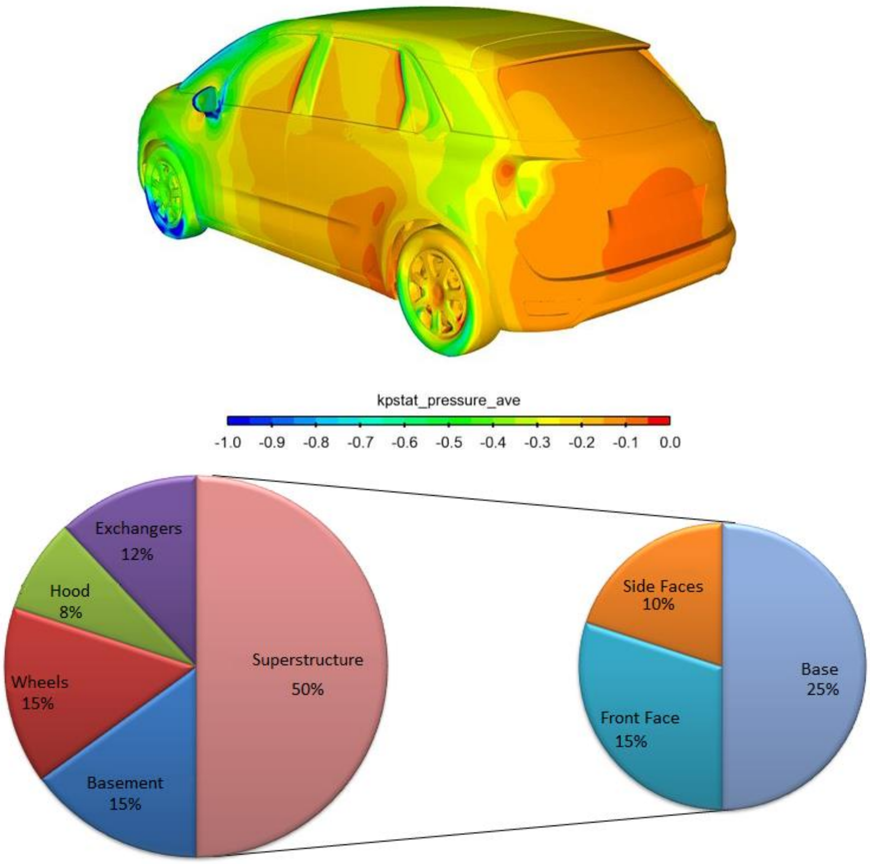

Figure 3-1: Top-side Cp distribution on a production vehicle; bottom-side different contributions of vehicle's parts to the pressure drag ([5]) .

Figure 3-1 shows that the wake contributes the most to the pressure drag. For this reason, in this work, we will focus on the car's base to have the greatest impact on fuel consumption and car emissions. With a view to improve and optimise the car’s wake, it is important to understand its dynamics and the flow behaviour in it. Figure 3-2 and Figure 3-3 show the three major turbulent flow structures which can dominate the car’s wake and the symmetry plane velocity distribution.

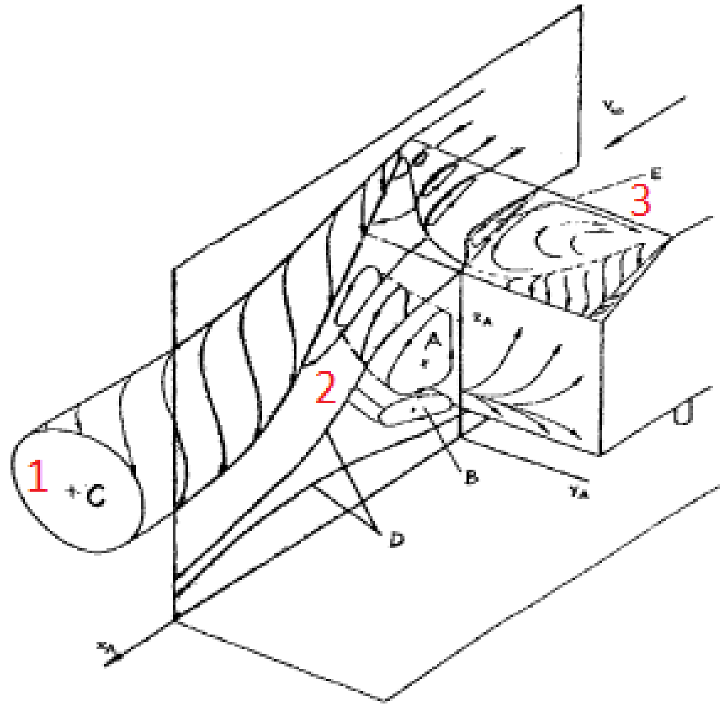

Figure 3-2: Dominant vortical structures of an academic body simulating a car ([12]).

The physics of a car wake is far from obvious. However, we use a simplified diagram of an academic body to understand the behaviour of the wake. Thus, we can see three dominant vortical structures in Figure 3-2. These three structures produce almost all of the drag generated by the wake, and therefore, it is crucial to act on them to have remarkable effects in terms of drag reduction. Structure number 1 represents the longitudinal vortices. They are generated where the side window ends and where there is a clear separation of the flow; these vortices are more or less intense depending on the flow separation and the flow structure at the base of the vehicle. Structure number 2 is called recirculation torus. It is generated because of the massive detachment of the flow due to the car's movement. The detachment generates an area of depression which allows the fluid's recirculation. Structure number 3 is called separation bubble, and the physics is similar to structure number 2 except that in this case, the detachment does not involve the whole surface of the rear window. In fact, there is a partial detachment with a consequent reattachment of the flow, which makes the shape very similar to a bubble, hence the name recirculation bubble.

Overall, these structures introduce vorticity into the flow, causing increased drag. In order to be able to reduce drag, it is, therefore, necessary to control these dominant vortical structures by trying to remove or weaken them. However, it is not easy to control these structures since we are talking about non-linear and unsteady phenomena. Moreover, in the case of real cars with square-like bases, the flow can show bi-stable behaviour for certain yaw angles, as shown by [9] and [13]; thus, the flow physics becomes even more complicated. Besides, when the yaw angle increases, the wake is no longer symmetrical. All these aspects increase the complexity of the flow and make it difficult to understand.

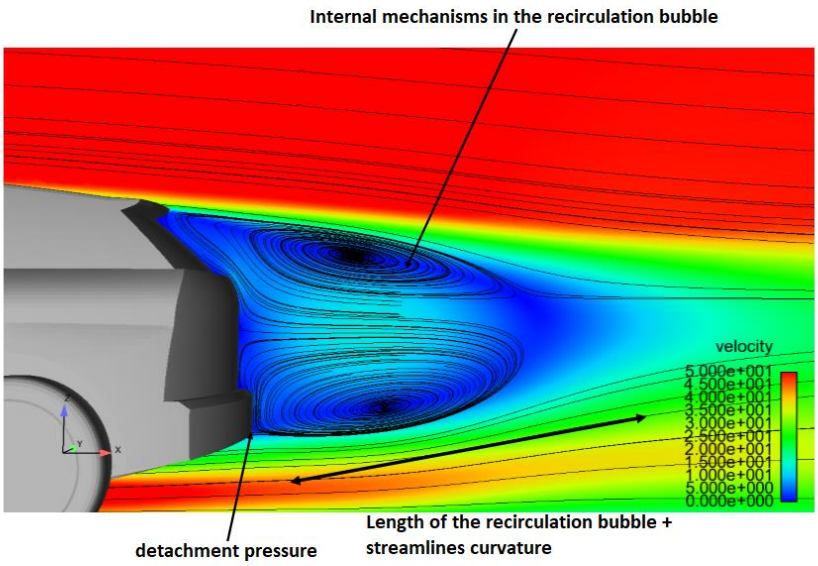

Figure 3-3: Velocity distribution and streamlines of the flow on the symmetry plane of a car's model([8]).

In our specific case, as shown in Figure 3-3, structure number 3 does not exist because of the sharp geometry of the blunt body. Besides, structure number 1 does exist, but doesn't contribute massively to the drag of the vehicle (vertical base). Hence, the number 2 becomes the most important structure. The thick body generates a massive detachment, and therefore, the recirculation zone is created. The length of the recirculation zone modifies the curvature of the streamlines. They are important because they generate the pressure field on the base, which is indicative of what is happening on the rear side of the vehicle.

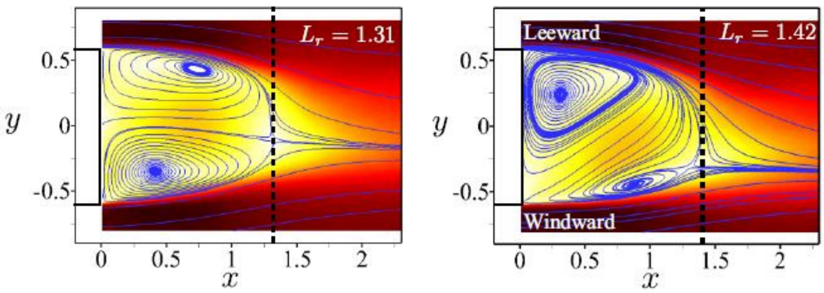

Figure 3-4: Top-side view of an Ahmed's body wake; On the left-hand side the flow is aligned with the symmetry axis, on the right-hand side we have a non-zero yaw angle ([14]).

The yaw angle strongly modifies the streamlines and the recirculation torus, which leads to an increase of drag directly linked to the incident flow.

Ideally, one wants to optimise a car by designing a symmetrical silhouette that produces the least drag for a zero-yaw angle. Still, a car produces very complex flows to understand. Moreover, studies, as well as tests carried out on the road ([2]), show us that, on average in real cases, the incident flow is almost always subjected to a non-zero yaw angle, as pointed out by [1] and [12]. For this reason, we need to understand the behaviour of the flow around a car according to the environment that surrounds it (urban environment, traffic, motorway, forest, etc.). Therefore, we want to understand the correlation between the incident flow and the pressure at the car's base.

Figure 3-5 shows the variation in the yaw angle observed during a road test at Heathrow. ([1]).

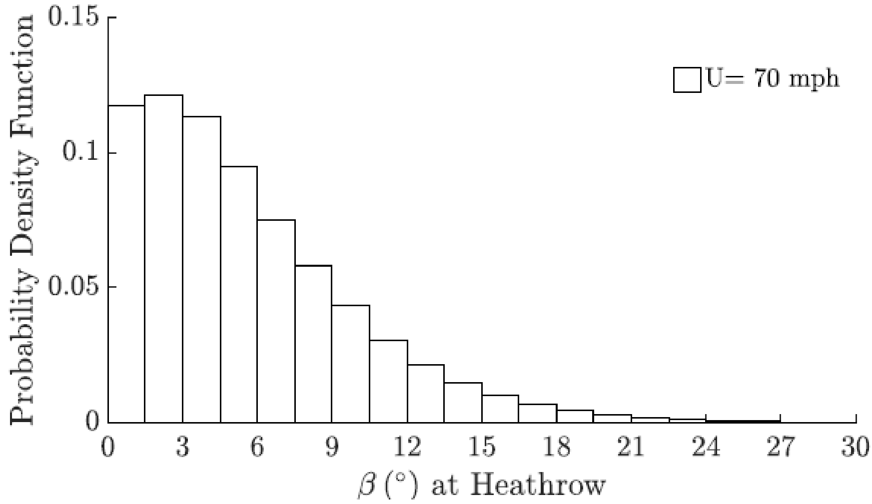

Figure 3-5: Probability density function of the absolute value of incident angles on a typical Heathrow route ([1]).

The behaviour appears very clear; we only have a zero-yaw angle for about 12% of the route on the analysed path. We can deduce that, on the remaining 88% of the way, we are subject to a non-zero yaw angle between ±20°. As the probability of having angles greater than 10° is low, we have chosen to concentrate ourselves on angles between ±10°. It is essential to define the convention used from now on; we illustrate it in Figure 3-6 and is the same one used in the tests carried out at the GIE-S2A (wind tunnel described earlier in chapter 2.2).

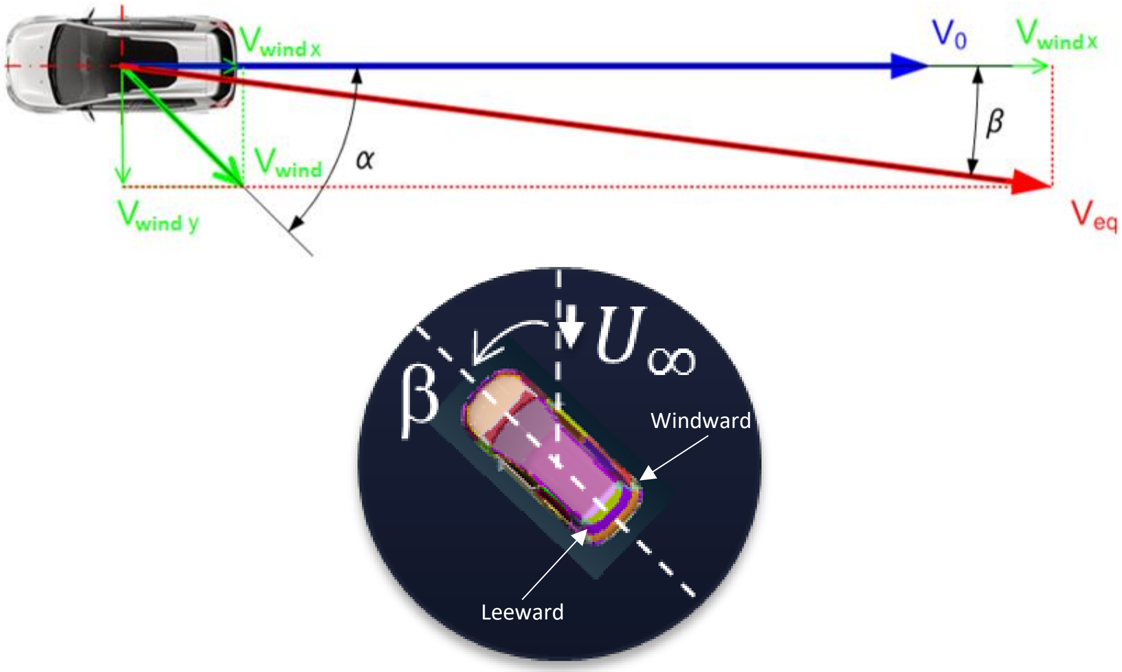

Figure 3-6: Convention used for the yaw angle.

In the upper part of Figure 3-6, we can see how the yaw angle β is defined. It depends on the wind component, which changes the equivalent speed (V_{eq} in Figure 3-6). In the lower part it is possible to see the convention used in the study of flaps' effects on the wake.

At present, many researchers are studying optimal solutions that can limit the problem and thus reduce drag. We can find very interesting active or passive solutions ([15], [16], [17] and [12]). There is a huge difference between these solutions; the active solutions, which can be jets or mobile flaps, seek to optimise the wake at every moment. In contrast, the passive solutions are devices that do not move, such as flaps, so these devices have an average gain in terms of drag, but this gain is not the optimal one at any moment.

In this work, we will study in detail the behaviour of a car's wake in static conditions, more precisely with flaps placed on the rear window. This work is the continuation of an internship preparing a doctoral thesis on active drag reduction where we will study controlled solutions.

For the reminder, we will focus more on passive drag reduction solutions to build a database for the doctoral thesis. In this respect, there are many references to studies ([1], [12], [18]) on academic bodies. These studies show the beneficial effects of specific aerodynamic devices, such as flaps positioned on the base of Ahmed's modified bodies. These devices act on the dominant structures (Figure 3-2) by adjusting the base's pressure field. They can be aligned with the body or inclined, so it is crucial to define the convention used in this specific case.

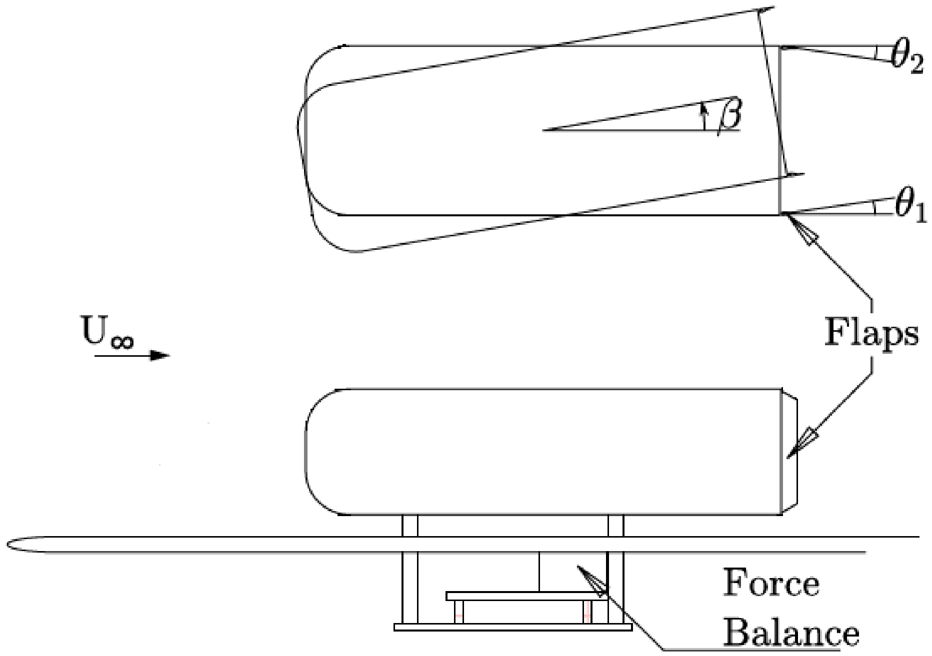

Figure 3-7: Convention used for the inclination angle of the flaps ([1]).

Figure 3-7 shows the convention used by [1], which we will also operate during our tests. We can distinguish the yaw angle β as well as the flap angles θ_1 and θ_2. These latter are considered equal to 0° if the flaps are aligned with the rear quarter (lateral surface of the model). In contrast, they are considered positive if they are inclined inwards (towards the rear window) and, vice versa, they are considered negative if they are inclined outwards.

The angles we have just defined are essential because they play a key role. [1] and [15] show that, depending on the flap's inclination angle, there is a more or less important gain, so they have highlighted the existence of an optimal configuration for each yaw angle. However, it is essential to define a new concept of the windward and leeward flap (terminology to indicate the flap that is most exposed to the flow and the one that is least exposed to it) because there is a big difference in terms of optimal angles. If a flap is windward, it has a significant influence on the wake. Therefore, a change in the angle of the windward flap produces a major variation in the wake. Conversely, the leeward flap has a smaller influence. Therefore, a variation of the leeward flap's angle produces a small variation in the wake of the car.

The presence of these flaps weakens the vortical structures in terms of vorticity intensity. As a result, the overall drag is reduced. However, as the flaps are fixed, they do not always provide the optimal configuration, as shown in [1].

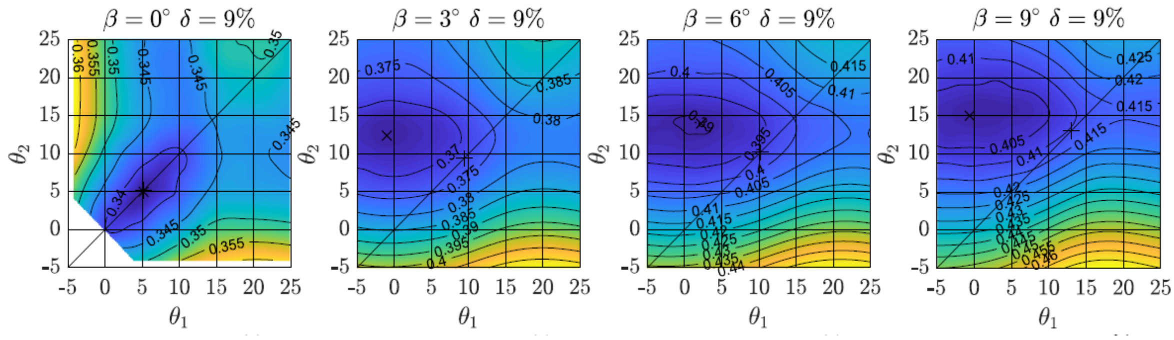

Figure 3-8: Optimal flap's inclination according to the yaw angle β ([1]).

In Figure 3-8, the importance of the flap's angles is noticeable. First of all, it is necessary to define the analysed parameters. β corresponds to the yaw angle, δ to the length of the flap in relation to the width of the model, θ_x to the flap's inclination angle, and we can specify that in the analysis carried out by [1], θ_2 is always the angle of the windward flap. We cannot have fixed flaps and at the same time having always an optimal gain. Therefore, we thought of first studying the wake's behaviour as a function of the flap angles and then moving on to adaptive aerodynamics.

3.1.1. Starting point and progress

My internship follows another one (Clément Melin's traineeship [8]), where we were able to start studying certain aspects in the wind tunnel. According to the bibliographical research we made, we could understand that the flaps, placed in continuation of the side window, bring a significant gain. Thanks to the tests already carried out, it has become clear that the thickness does not play an essential role. We also validated the results shown in Figure 3-8. We can say that the beneficial effect due to aerodynamic devices is also present in a non-academic model, such as the one tested in the wind tunnel. During my work, several activities took place, especially of experimental nature. The practical tests took place in the wind tunnel, at the GIE-S2A described above (Chapter 2.2).

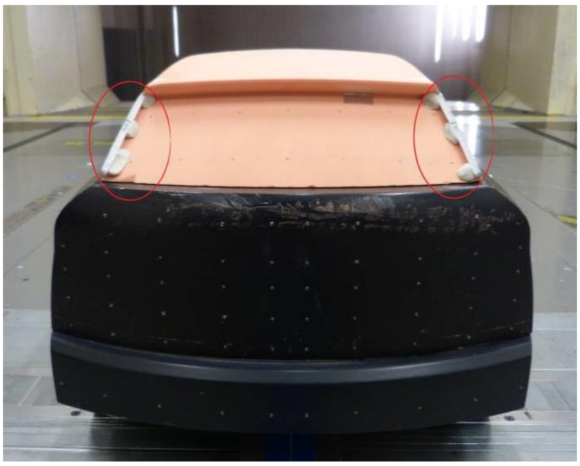

Figure 3-9: Cross-Hatch SUV with a symmetrical flap configuration ([8]).

Figure 3-9 shows the model that has been used up to this point by my company's tutor. Due to a problem we had and to allow better test repeatability, we designed a new rear cabin for this model, with CATIA V5 (we give more details about the design in Chapter 4). The different flap configurations were also developed in CAD, again to allow test repeatability.

4. Design of the devices to be tested

4.1. Initial condition

At the beginning of my internship, there was a LAB milling model shown in Figure 4-1.

Figure 4-1: On the left-hand side, in orange, the rear cabin in LAB milling SUV type; on the right-hand side an example of flap ([8]).

Due to an erroneous speed-yaw configuration, i.e. too high speed in relation to the imposed yaw angle, as well as wear and tear on the part, during a wind tunnel test, the rear cabin detached and was consequently destroyed. This meant that the model was no longer usable and so we had to think about adapting to the situation so that our study could continue. To do so, we thought of redesigning it, using CatiaV5, to produce a rear cabin and several flap models in additive manufacturing. This modular rear cabin allowed us to integrate additional functionalities, such as flaps, different spoiler types and pressure tappings. All this would have had to be done by hand in the case of the old LAB milling rear cabin, an aspect that would have added source of error.

4.2. CAD numeric models

The starting point is the surface model shown in Figure 4-2, also representing the model from which the LAB milling rear cabin was produced.

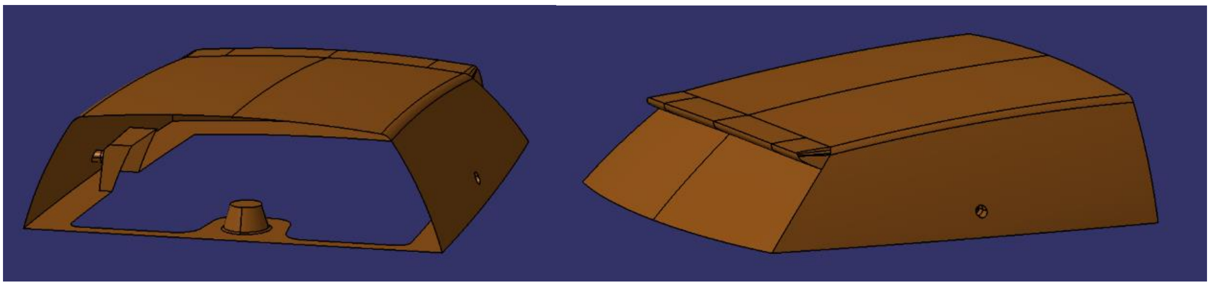

Figure 4-2: Surface starting point for CAD.

The visible holes are used to fix the rear cabin to the bracket. In this case, the spoiler forms a single body with the rest of the part. As a LAB milling model, it was easier to make holes for pressure tapping and fit inserts to allow the flaps to be fixed after digging out the foam. Since additive manufacturing products are much more robust, they do not allow this solution so easily without the risk of cracking the model. For this purpose, all sensitive points had to be provided, i.e. points for pressure tapping, points for attaching the flaps, points for attaching the body to the existing model and points for securing the spoilers. Once we chose each point's correct position, we provided all the fixing systems and the holes to be made directly in the CAD.

The final result is shown in Figure 4-3.

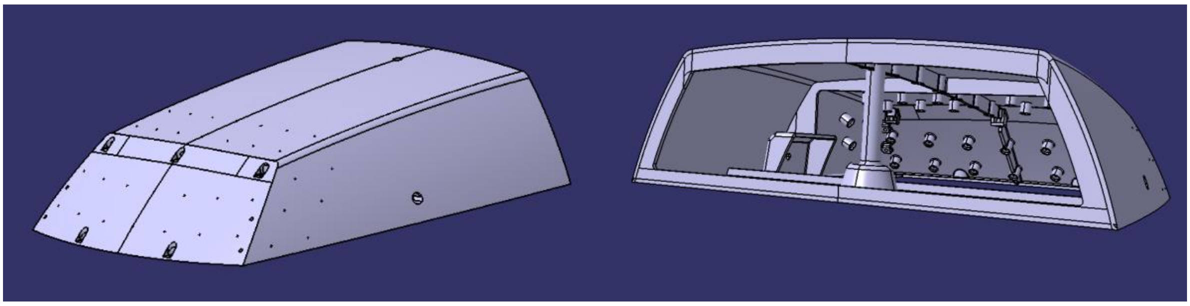

Figure 4-3: On the left-hand side the external part of the final model; on the right-hand side the internal part of the final model.

The initial surface model has been improved in certain aspects of construction which has allowed to have a rigid model and at the same time test repeatability, which is very important for this type of study. Below, we will discuss these aspects, and we will provide a critical look to justify the design choices.

4.2.1. Construction details

As the spoilers were already manufactured, in this model, we had to provide suitable fixings for the already designed systems. Figure 4-3 shows three indentations for fixing the spoilers in the upper part of the rear window. These are shown in detail in Figure 4-4.

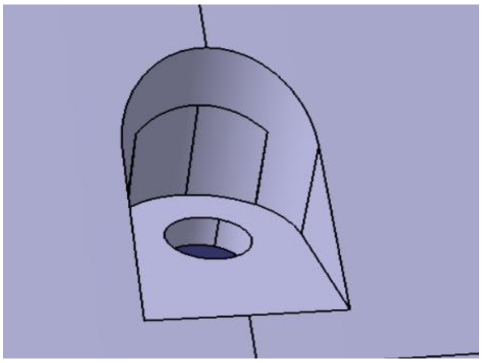

Figure 4-4: System for fixing the spoilers and also the model to the existing mould.

As one of the spoilers was already made, it was adapted to fit the model using this shape. However, we also used this impression to add fixing points between the rear cabin and the model using it simultaneously as a counterbored hole. We can see this type of fixing points at the bottom of the rear window in Figure 4-3 on the left-hand side.

Furthermore, if you look at the model from the inside you can see two ribs. They are highlighted in Figure 4-5.

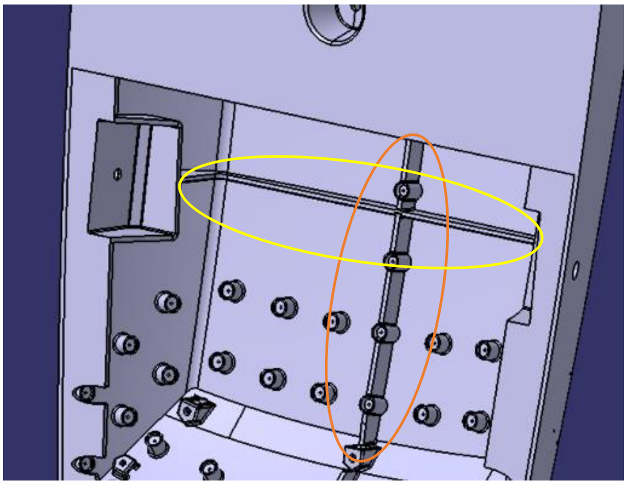

Figure 4-5: Ribs to stiffen the model.

As large surfaces, relative to the whole model, the parts representing the rear window and the model's roof are necessarily flexible. We thought of adding two ribs, a longitudinal one circled in orange and a transversal one circled in yellow, to deal with this problem. These two ribs make the entire rear cabin more rigid. Besides, still in Figure 4-5, we can see that the longitudinal rib has pressure tappings. So, we can see how they have been integrated into the rib. As a preventive measure, five additional pressure tappings have been placed along the rib's entire length, as it is challenging to drill it correctly and efficiently without the risk of cracking the model once it has been already manufactured.

Now, looking at the two side parts, we can see two holes and two supports which are shown in Figure 4-6.

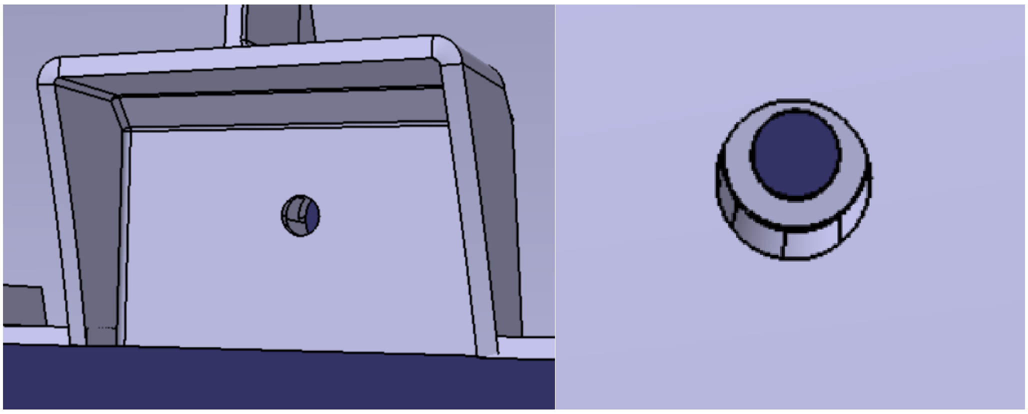

Figure 4-6: Details of the fastening system, respectively internal on the left-hand side and external on the right-hand side, which are placed symmetrically on both sides of the model.

The support on the left is simply the thickened surface of the surface model. Therefore, to fix the part, it is necessary to screw it in with an M6 screw. Since a screw is a factor of disturbance in the flow, it was preferred to hide it by using a counterbored hole. Once the part has been fastened, this type of spot is plugged with aluminium adhesive to make the surface as smooth as possible to not disturb the flow. A counterbored hole, to accommodate the screw head, must have a hole with a diameter equal to almost twice the diameter of the screw. Therefore, in this case, a diameter of 12 mm is considered.

Looking at the model from the front, we can see a tube connecting the conical shape to the roof of the model, as shown in Figure 4-7.

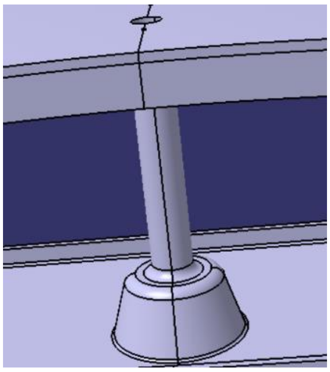

Figure 4-7: Detail of the cone-shaped fastening system.

To avoid the problem, we had with the foam model, we also looked for new fixing points, such as the holes on the rear window and the system shown in Figure 4-7. These points allow better fixing and therefore guarantee greater safety. However, the tube also plays another role. It is a counterbored hole that receives an M6 screw, but, simultaneously, being connected to the upper surface, it also helps to stiffen the structure. Therefore, it is an improvement of the original model.

As already mentioned before, the part in additive manufacture is stiffer in terms of material, so it is not possible to use inserts without (taking) the risk of cracking the model. For this reason, all the holes had to be provided in advance as well as the fixing systems. We thought of using a special shape that allows a nut to be fixed so that we could simply use a screw-nut system with a nut that is glued to the model. This shape and the pressure tapping are shown in Figure 4-8.

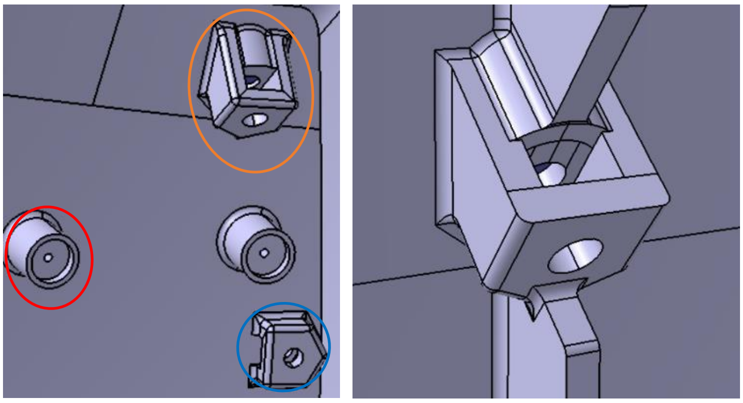

Figure 4-8: On the left-hand side nut fastening system circled in orange, pressure tapping circled in red and edge fastening system circled in blue; on the right-hand side implementation of the nut fastening system in the longitudinal rib.

We can see the nut fastening systems, surrounded in orange and blue. This particular shape allows a nut to be received and glued into it. Once the nut is glued in place, we can screw on and off. Therefore, this system is a substitute for the insert in the foam and fulfils the same function. In the right-hand part of Figure 4 8, it is shown how the fastening system has been implemented in the longitudinal rib as it corresponds to the hole in the middle of the rear window.

Besides, circled in red, we can note one of the pressure tappings. The shape used is designed so that the stainless-steel tubes can be inserted and glued while ensuring perpendicularity to the external surface. Simultaneously, the small recess is used to accommodate the glue and make it more difficult for it to come off.

As is well highlighted in Figure 4-3 and Figure 4-5, there are many pressure tappings, more precisely 45. All the tappings must be placed perpendicular to the wall to allow a correct measurement of the pressure, and therefore also the shapes must extend perpendicular to the wall. However, some of them conflict with the support at the bottom of the model, as shown in Figure 4-9.

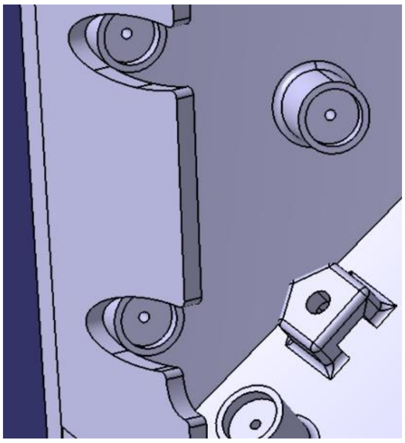

Figure 4-9: Conflict between pressure tappings and support at the bottom of the model.

As a result, the supports had to be re-cut so as not to obstruct the steel tubes. For the way the model was designed, and for the points chosen to measure the local pressure, there is little conflict between pressure tapping and the model's support.

In order to measure the pressure on the model, the tubes must be in contact with the flow. Therefore, we have tubes flush with the outer wall, as shown in Figure 4-10.

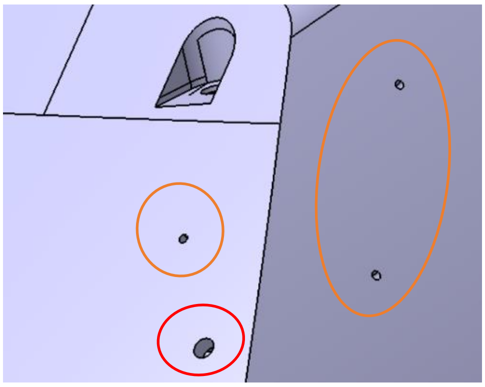

Figure 4-10: Detail of pressure tapping holes surrounded in orange and holes for flaps fixing surrounded in red.

Surrounded in orange, we can see the holes for the pressure tapping. The tubes go up to the surface and do not come out so as not to disturb the flow enormously. Besides, surrounded in red, we can see the hole for fixing the flaps (encircled in red in Figure 4-12 and the Glossary) with an M3 screw. Behind these holes, there is the fixing system analysed in Figure 4-8 on the left and circled in blue.

4.3. CAD of the reference spoiler and flaps

4.3.1. Reference spoiler

The spoiler that constitutes the reference, being one body with the previous foam model, has broken. Once the rear cabin was designed, the reference spoiler also had to be produced. In this case, the spoiler was created by thickening the surface model, shown in Figure 4-2, and adding the three male shapes that fit the rear cabin's attachment systems (Figure 4-4).

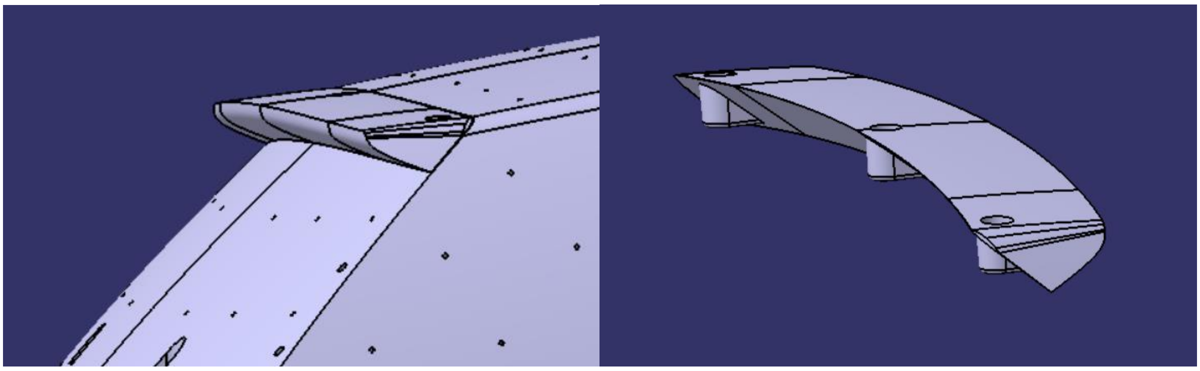

Figure 4-11: On the left-hand side the reference spoiler integrated in the rear cabin; on the right-hand side the reference spoiler.

Figure 4-11 shows the result of the CAD-designed reference spoiler. In addition, it can also be seen directly integrated into the similarly designed rear cabin.

4.3.2. Flap’s designs

As explained before, on the model, some holes allow the placement of flaps. These have also been designed in CAD to produce them in additive manufacturing. In this case, the flaps are not part of the same body, and therefore they are analysed below.

It is important to understand what a flap is and where to place it. We can see it as an extension of the model's side surface. Therefore, it is placed on the rear window, as shown in Figure 4-12.

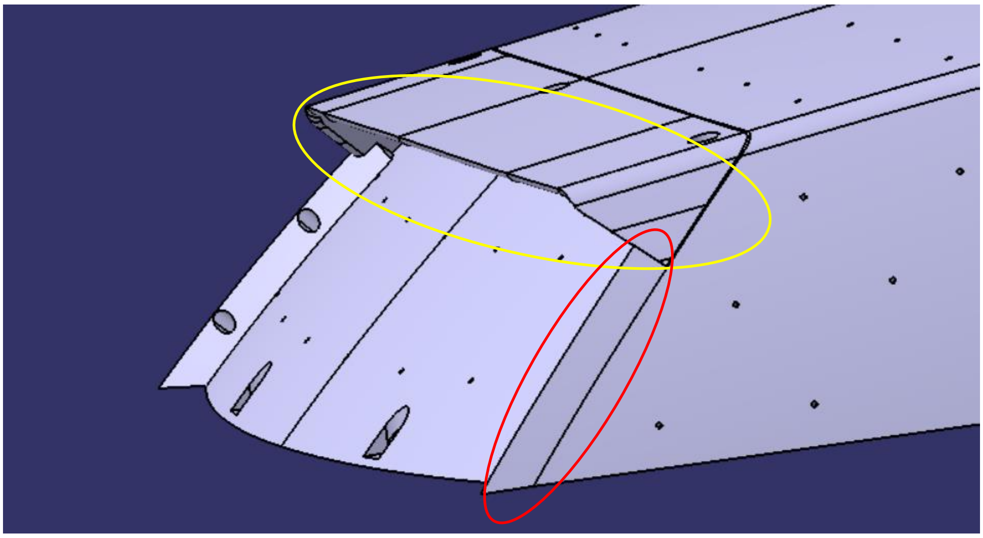

Figure 4-12: Rear window with the flaps, circled in red, and the spoiler circled in yellow.

In Figure 4-12, two aerodynamic devices are highlighted, the flap encircled in red and the spoiler encircled in yellow. Only the flap will be analysed in detail afterwards.

In order to understand the effect of the flaps, it is essential to understand what role all the parameters play, i.e. flap's length, thickness, and inclination. We can do this by varying these parameters to produce several flap configurations. The thickness has already been tested, so now we want to analyse the inclination. It is important to understand how the angle is measured, and therefore the convention is explained below. The zero inclination, i.e. the flap angle equal to 0°, corresponds to the flap that extends the model's side window. Positive angles correspond to the flap inclined inwards, i.e. approaching the rear window. On the other hand, negative angles correspond to the flap tilted outwards, i.e. away from the rear window (Glossary).

Several inclinations are to be tested. More precisely, we want to analyse already tested configurations to have a clear idea and compare the results already obtained with the new ones. So first we are thinking of producing four different flap configurations, more precisely the 0°, 8°, 16° and 24°. Secondly, in accordance with the bibliography, especially [1], it has been proven that there is an optimal inclination depending on whether the flap is windward or leeward (Figure 3-6). Tests have shown that there is an optimum for static configurations. This optimum is placed around 15°. We may produce other flaps with inclinations between 10° and 20° outside this internship context.

The design choices are detailed afterwards.

4.3.3. Construction details

We had to adapt the flaps to the existing models; more precisely, we had to bend them to follow the model's side window's curvature. We also had to cut the flaps so that the spoilers could be fitted easily. We can see details of the flap adaptations at the spoiler's corners in Figure 4-12.

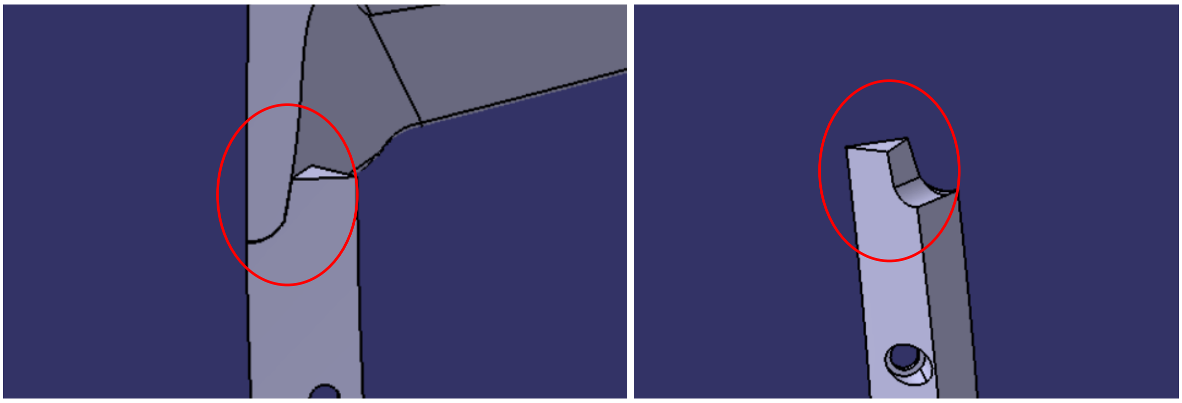

Figure 4-13: Adaptation of the flaps to the spoiler's corners.

Figure 4-13 shows how the flaps had to be adapted and how they had to be designed with this shape that fits very well with the spoiler corners.

Another interesting detail is the counterbored hole; in fact, this type of hole makes it possible to hide the screw and thus reduce the fastening system's influence on the flow. We can see this detail in Figure 4-14.

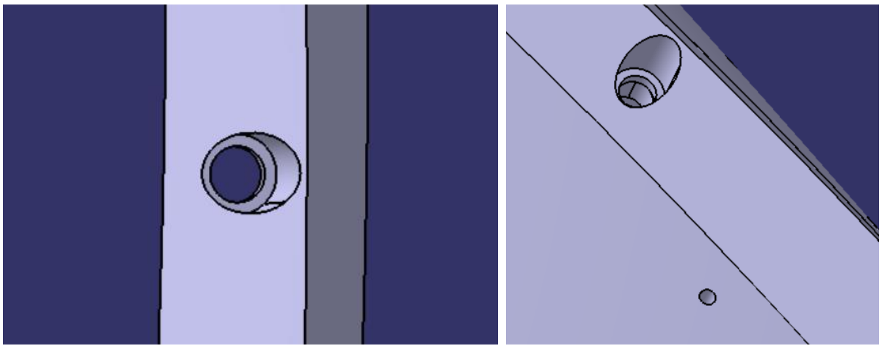

Figure 4-14: Counterbored flap holes and proximity to pressure tappings.

An attempt was made to place the hole in the flap's inner part, as shown on the right-hand side of Figure 4-14. However, this is not always possible because it is impossible to increase the flap's thickness since some pressure tappings are nearby and they cannot be plugged. Therefore, as the angle increases, the hole also touches the outer part of the flap. The counterbored hole, as mentioned above, allows hiding the screw.

At the bottom, the flap should be as close as possible to the existing model. Figure 4-15 shows the bottom of the flap.

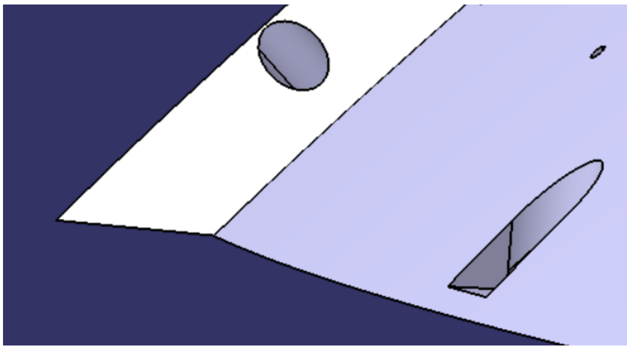

Figure 4-15: Bottom of the flap in contact with the existing model.

Overall, this form makes it possible to limit losses in this area.

The second counterbored hole at the bottom of the flap also needs a screw-nut fixing system, identical to those seen in Figure 4-8. However, there are more constraints in this case, as the hole is placed at the bottom, and here we also have the model support visible in Figure 4-5 and Figure 4-9. For this reason, it had to be designed differently.

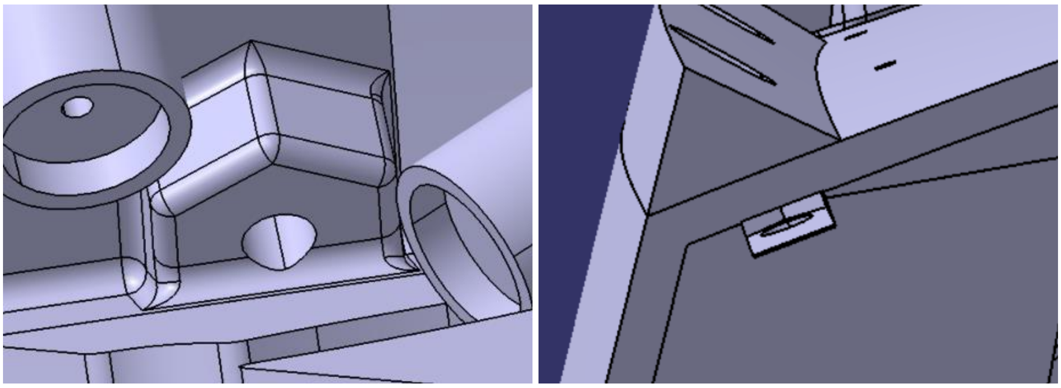

Figure 4-16: Screw-nut system for the hole at the bottom of the flap.

In Figure 4 16 on the left-hand side, we can see that the system is very close to the support at the bottom. Therefore, the fixing system and the support had to be fused together with the hole underneath the model in order to be able to insert the nut, as highlighted in the right part of Figure 4-16

Having two holes, for fixing the flaps, is very important. We guarantee that the flap does not rotate, and it ensures that the flap follows the shape of the rear window. Therefore, we provide the continuity of shape. This may not be guaranteed without the two fixing points, as the production process may generate errors due to the machine's tolerance itself.

Moreover, by having several flap’s inclinations, they can be easily distinguished on the digital file. However, once the flaps have been produced, it is not easy to distinguish the configurations, especially if we are talking about relatively close designs, i.e. 15° and 16°. In order to overcome this problem, we have chosen to mark the angle on the flap itself, as shown in Figure 4-17.

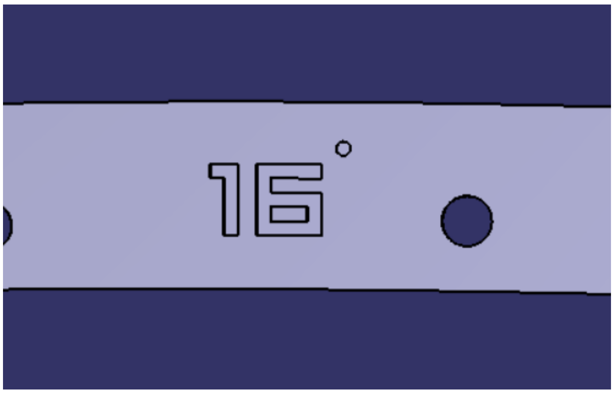

Figure 4-17: Example of 16° marked flap.

In this case, there is an example of the flap inclined at 16°. With this solution, flaps with a known angle of inclination are always distinguished.

4.4. Results and parts produced

After each part has been analysed in detail, the whole is put together, and we can see the result in Figure 4-18.

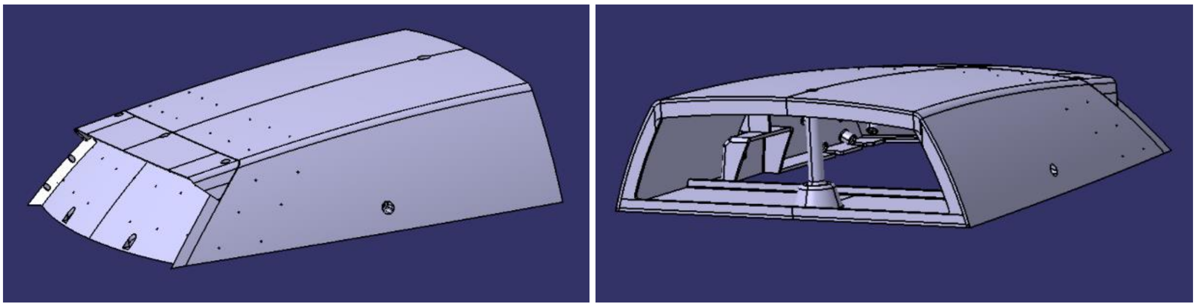

Figure 4-18: Complete body including spoiler and flaps.

It is worth noting that the flaps and the spoiler integrate well with the model, with no interaction between them and the rear cabin.

The dedicated department took the order and started the production of the rear cabin in ABS-M30. The software gave us an overview of the result and an order of magnitude in terms of time to produce it.

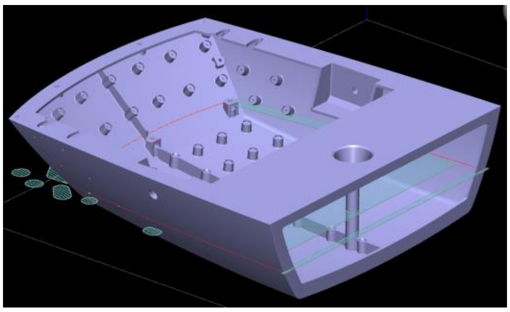

Figure 4-19: Overview of the result in additive manufacturing.

In Figure 4-19, we can see the overview that the production software gave us. The production time given is of the order of 91 hours, approximately four days continuously.

Figure 4-20: Repair of surface defects in the rear cabin.

The rear cabin had some imperfections, especially concerning the surface condition. These imperfections could have impacted the wind tunnel tests, so the model had to be puttied and sanded to make the surface as smooth as possible (Figure 4-20). The surface imperfections were caused by the orientation of the model in the 3D printer. The horizontal direction was chosen, which allowed us to have the rear cabin more quickly, but this choice meant that the surface condition was not optimal. The best orientation for our part was vertical. After puttying and sanding, the result is as shown in Figure 4-21.

Figure 4-21: External surface of rear cabin in ABS-M30.

The surface now appears smooth and clean (Figure 4-21). Overall, the rear cabin fits nicely on the foam model. Besides, on the left-hand side, we can see that the screws are inserted. This has been done to allow the nuts to be glued into the fastening system, shown previously in Figure 4-8 surrounded in orange.

Figure 4-22: Internal part of the rear cabin in ABS-M30.

Also, in Figure 4-22, we can see that the tubes for the pressure measurement have already been placed and glued. In Chapter 5, we will see in detail how these tubes will be used.

Firstly, we tested that the existing spoiler fits correctly on the rear cabin. The result is shown in Figure 4-23.

Figure 4-23: Existing spoiler mounting on the rear cabin in additive manufacturing.

The spoiler fits well, so we can test the other devices we have designed.

The reference spoiler and flaps are made of polycarbonate. The spoiler requires a production time of about 4.5 hours and the flaps about 0.5 hours each, for a total of about 8 hours of continuous work.

First, in Figure 4-24, we present the reference spoiler.

Figure 4-24: Polycarbonate-product reference spoiler.

We can see that the colour is different, but this is only due to the used material. Despite the change in material and colour, the reference spoiler is not defective, and it fits nicely on the rear cabin as shown in Figure 4-25.

Figure 4-25: Reference spoiler mounted on the new rear cabin produced in additive manufacturing.

We now analyse the production of the flaps and the assembly. In Figure 4-26, we can see the four different flap's inclinations.

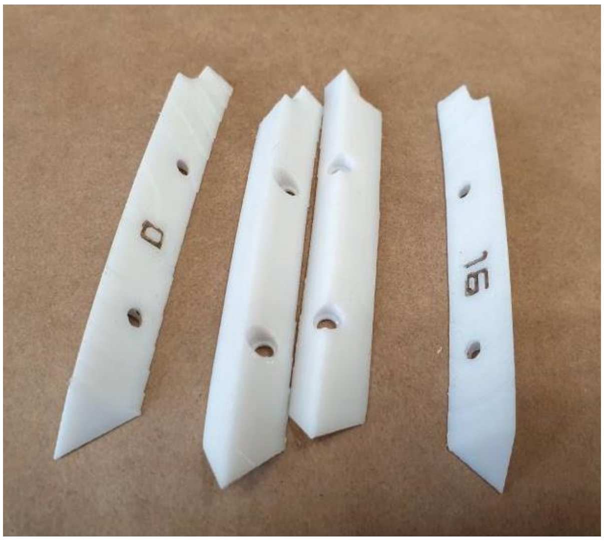

Figure 4-26: Different flap inclinations.

We can notice that the flaps' numbering is useful; it is visible on them for the 0° and 16° inclinations. The other two flaps are turned to the other side to have a 360° view. The curved part at the top of the flaps is used to fit the EVO spoiler that has already been made, as shown in Figure 4-27.

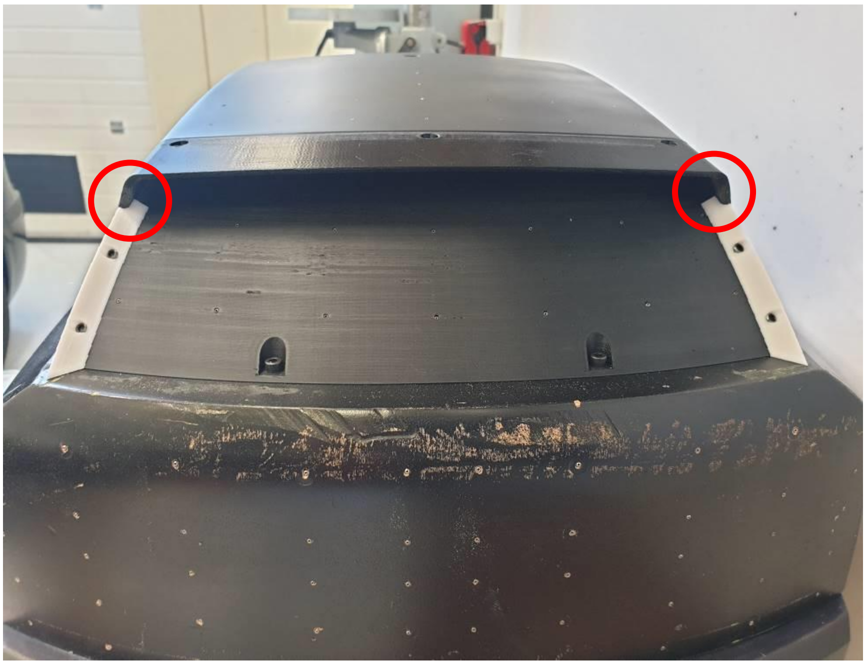

Figure 4-27: Existing EVO spoiler with flaps.

It can be seen that the flaps fit correctly and at the same time adapt well to the spoilers, in particular, we can see in Figure 4-27, circled in red, how the upper part of the flaps adapts to the shape of the spoilers.

Overall, the production results are satisfactory and meet all the requirements imposed during the design process. We now want to understand whether these ideas are functional in improving the cars' aerodynamic performance. To do this, we need to test these devices in the wind tunnel. The results will be detailed in Chapter 5.

5. Instrumentation of the model and wind tunnel tests

Once the pieces have been produced, it remains to prepare the tests by writing the session's programme. Besides, we must instrument the model so that we can test it in the wind tunnel. To describe the tests carried out on a reduced scale, we need to understand what we have to prepare before the session. Overall, what we want to measure corresponds to aerodynamic torsor (load set) and pressure coefficient (C_p) measurements. The balance under the wind tunnel plenum, described in subchapter 2.2, can be used to measure the torsors. However, to measure the Cp, the entire model must be instrumented with strategically placed pressure tappings. For this purpose, first, we will describe the process of model instrumentation in detail, and secondly, we will describe the wind tunnel tests.

5.1. Instrumentation of the model

As a new rear cabin was designed with a higher number of pressure tappings than the old model, the location of these tappings on the scanner also had to be changed. Finally, due to the high number of pressure tappings, we decided to use two pressure scanners and an analogic pressure sensor. Before detailing the scanners' connection, it is necessary to recall what the C_p is and why it is worth measuring it.

5.1.1. Pressure coefficient measurement

The Cp is a dimensionless pressure coefficient that gives us an idea of the pressure field around specific model's points. It is defined as follows:

$$C_p = \frac{p - p_{ref}}{\frac{1}{2}\rho V_\infty^2}$$

Where:

- p is the measured pressure at the chosen point
- p_{ref} is the static reference pressure, here we consider the upstream static pressure
- $\frac{1}{2}\rho V^2_\infty$ is the dynamic pressure Q_∞ with ρ the fluid's density and V_∞ the upstream flow speed.

To calculate the Cp, all these parameters need to be measured. The dynamic pressure Q_∞ and the reference pressure p_{ref} are measured automatically using static pressure tappings in the nozzle, as shown in Figure 5-1. According to a GIE S2A document [19], both parameters are calculated as detailed in Figure 5-1.

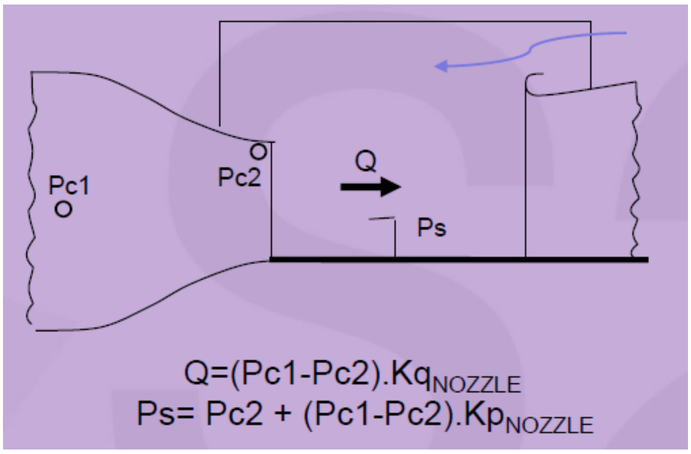

Figure 5-1: Method for calculating the dynamic pressure and the reference pressure, respectively Q and P_s ([19]).

However, as the flow acceleration depends on the convergent, and as the latter is indirectly related to the dynamic pressure, a correction factor associated with the convergent must be considered, which in this case is $K_q = \frac{Q_{actual}}{Q_{measured}}$. This correction factor has been calculated by measuring the $Q_{measured}$ in the vein and the Q_{actual} on a model in the plenum using a pitot tube placed at the front of the model. With this information and using the formula in Figure 5-1, the Q used to calculate C_p is obtained. In the same way, the correction factor K_p, related to the pressure, was calculated. Using the formula in Figure 5-1, it is possible to calculate the p_{ref}.

To obtain the C_p, we only need the value of the static pressure at the chosen point. It is measured using steel tubes placed in the pressure tappings illustrated in chapter 4. The (p - p_{ref}) value is calculated using a Scanivalve ZOC 33 differential pressure scanner with 64 channels, connected to Scanivalve DSM conditioning electronics. The instrumentation of the model, with the steel tubes and the useful vinyl to transfer the information, is detailed below.

5.1.2. Installation of steel tubes and vinyl

The entire model has a total of 107 pressure tappings, more precisely 62 placed on the model in LAB milling (Figure 5-2) and 45 on the rear cabin in additive manufacturing (Figure 5-3).

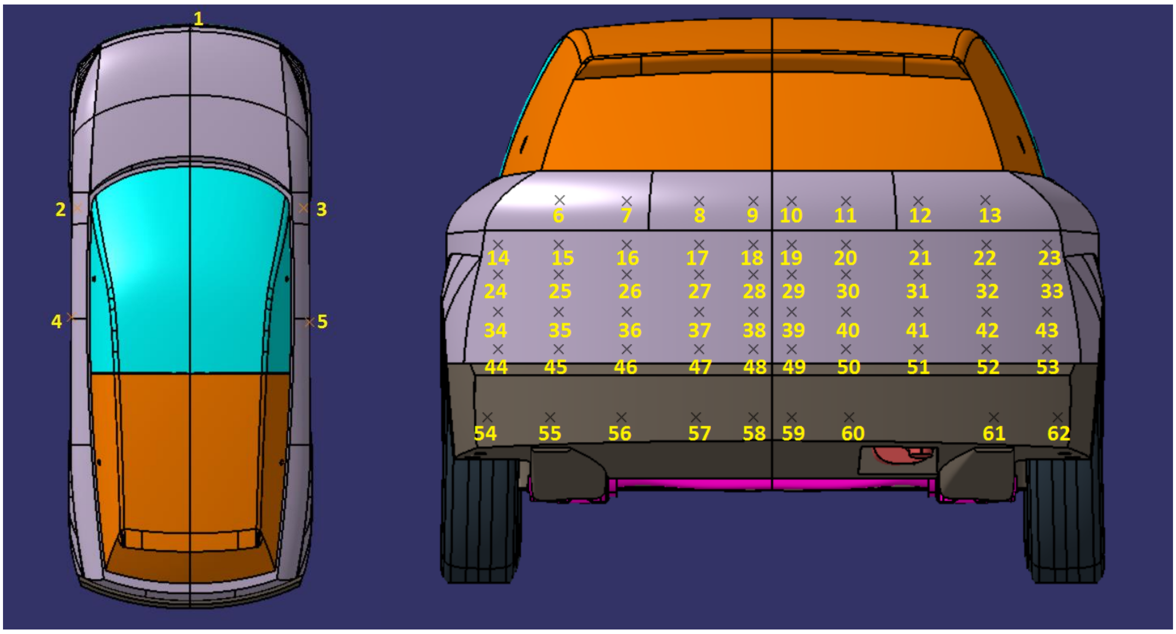

Figure 5-2: Pressure tappings on the LAB milling model.

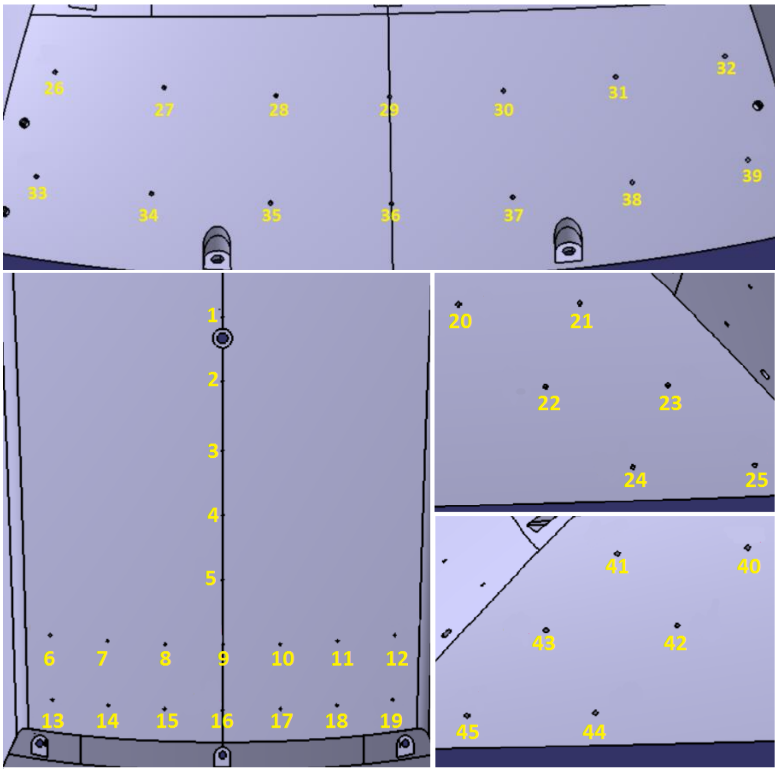

Figure 5-3: Pressure tappings on the rear cabin in additive manufacturing, at the top-side the rear window and at the bottom-side the roof and the two rear quarter panels.

The LAB milling part has already been used previously by my tutor and some colleagues, which is why the pressure tappings were already present. We only had to double some of the tappings to have redundant information on both scanners. We did this to "realign" the two different scanners we used. Besides, channels 2 and 3 were averaged to use the value also in an analogic sensor. In our case, this sensor aims to measure the value of the dynamic pressure Q on our model during the tests to increase the test repeatability. The analogic sensor is shown in Figure 5-4 encircled in red.

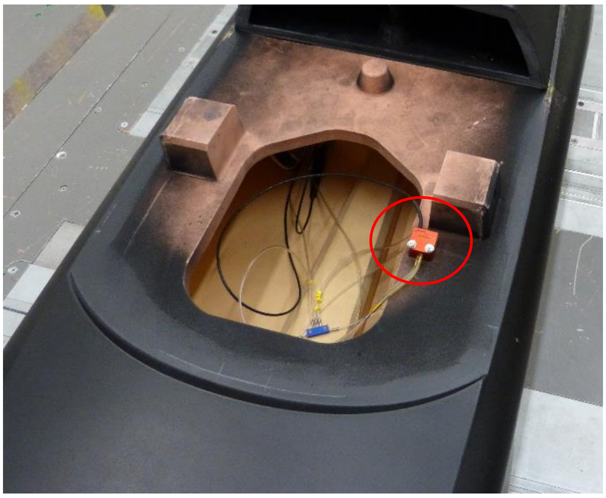

Figure 5-4: Analogic sensor for measuring the value of Q.

The most important part of the instrumentation concerns the rear cabin. The steel tubes have an external diameter of 1.6 mm and an initial length of 1 m. For this reason, the tubes had to be cut into 45 pieces long enough to be flush with the outer wall. Simultaneously, they had to be of the correct size to be glued into the additive manufacturing supports (piece encircled in red in Figure 4-8). Before cutting the tubes, sandpaper was passed over the external surface, to have a surface that interacts better with the glue. After cutting the tubes, the friction between the abrasive disc and the tube itself generates burrs on the cut end, both inside and outside the tube. The tube pieces were deburred using special tools. To make sure that there were no residues inside the tubes and to degrease them for bonding, they were placed in a solvent. They must now be dried and set correctly. The final result is shown in Figure 5-5.

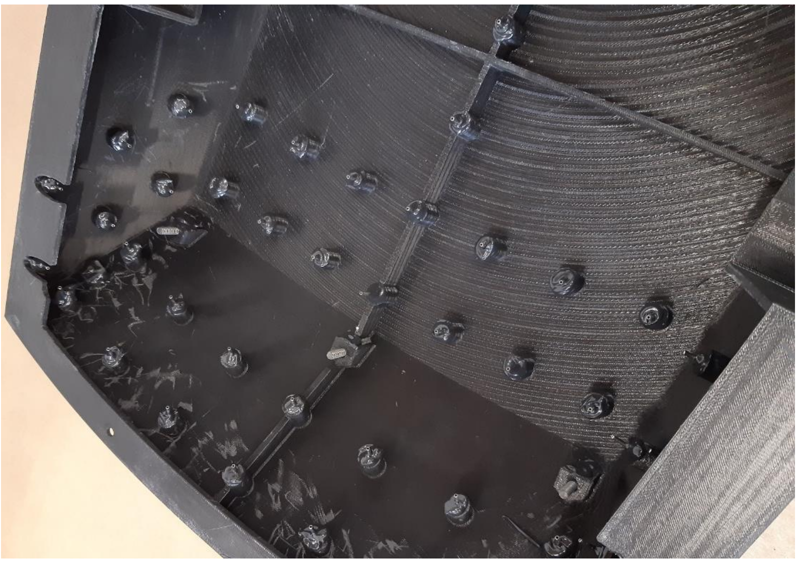

Figure 5-5: Result of steel tubes placement for pressure tapping.

The information must now be transmitted from the tubes to the connectors that connect to the scanner. Vinyl tubes were used for this purpose. These tubes have been numbered to be able to intervene more quickly in case of problems with the pressure tappings. The result of the vinyl placement is shown in Figure 5-6. These vinyl tubes were connected to a Scanivalve 48-way connector ([20]) connected to the scanner when the pressure is to be measured during a wind tunnel test.

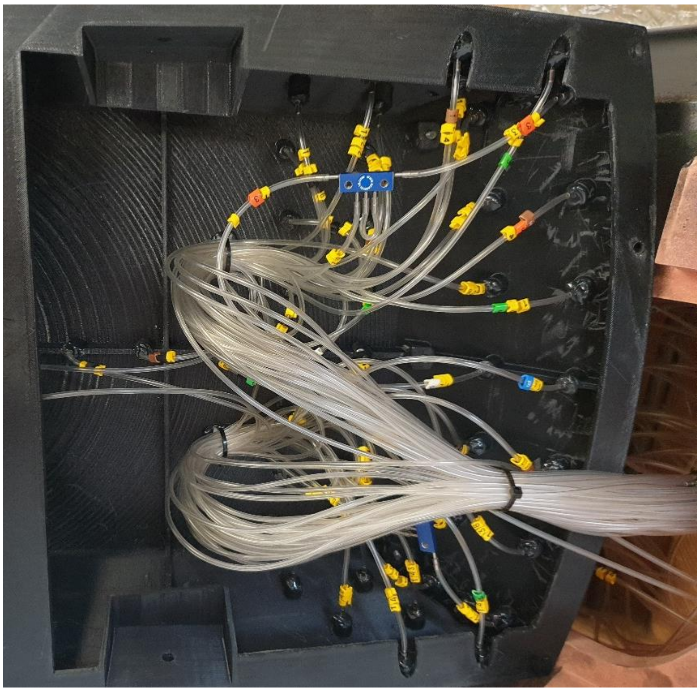

Figure 5-6: Placement of numbered vinyl tubes to transmit pressure information.

5.2. Wind tunnel tests

Once the model is instrumented, wind tunnel tests of the various components must be carried out. It is possible to directly measure the aerodynamic forces by means of the force balance and carry out pressure measurements. Due to the large number of configurations to be tested, it was impossible to carry out tomography due to lack of time (only 3 days of wind-tunnel test campaign). First, we will illustrate the convention used, and then we will analyse the results in terms of aerodynamic torsors and pressure coefficients.

The model used is modular, the rear cabin, for example, can be changed. We have an SUV type rear cabin, like the one we will analyse in this work, and a fastback type rear cabin, like the one used in the work carried out by [8].

Subsequently, our study will focus on the rear part of the vehicle and therefore more specifically on the base, roof, spoiler, rear quarter and flaps (Glossary).

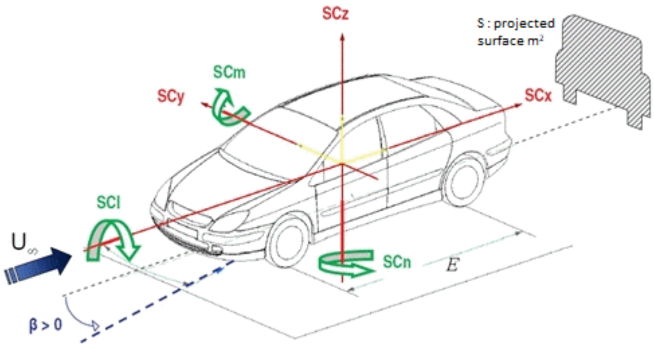

Figure 5-7: Convention used for aerodynamic torsors ([21]).

Figure 5-7 shows the convention used in the subsequent analyses. The wind tunnel balance allows us to measure the forces and moments along the different axes using the formulas:

$$F_i = Q_0 S C_i \quad \text{and} \quad M_i = Q_0 S C_{mi} L_0$$

where:

- F_i is the aerodynamic force calculated according to the desired axis
- M_i is the moment due to the aerodynamic forces around an axis
- Q_0 is the dynamic pressure calculated using the fluid's density and the upstream flow speed
- S is the projected surface of the vehicle along the desired axis
- C_i is the dimensionless force coefficient along the desired axis
- C_{mi} is the dimensionless aerodynamic moment coefficient
- L_0 is the characteristic length for calculating the aerodynamic moment

First, it should be pointed out that the projected surface S is very difficult to measure precisely each time. For this reason, the SC_i and the SC_{mi} are calculated using the following formulas:

$$SC_i = \frac{F_i}{Q_0} \quad \text{and} \quad SC_{mi} = \frac{M_i}{Q_0 L_0}$$

The different values of the aerodynamic torsor are measured using the balance detailed in subchapter 2.2. If pressure measurements are carried out, the pressure differential values, measured with the scanner, are also provided.

5.2.1. Analysis of aerodynamic torsors and pressure fields

For the three days available in the wind tunnel, more than 250 runs have been programmed to measure more than 220 aerodynamic torsors. This means that all the configurations that we want to test must be correctly chained together, trying to minimise the parts to be assembled and disassembled between one configuration and the next. In the 250 runs, long acquisitions are also planned, i.e. time-series acquisitions lasting few minutes. These acquisitions make it possible to see the convergence velocity of the results, and therefore not only the torsor averaged over the last 80 seconds (the standard method of measurement of GIE-S2A). Thanks to this, it is possible to understand whether the flow around the model is unsteady or not. Besides, these runs also include the measurement of the C_p.

Fortunately, we didn't have any significant problem in the three days of testing, so the three sessions went as planned. This is an important aspect to consider; sometimes, it happens to have problems that have a substantial impact on the session, and therefore we need always to be ready to adapt quickly.

The model has been used several times in the past. However, by using the new rear cabin during these tests, it is planned to re-run specific configurations for cross-checking and validation purposes.

At the beginning of the first test session, the model must be installed in the vein. Four pawns fit into the four wheels of the model; this allows us to know that the model is aligned with the wind tunnel reference. Figure 5-8 shows the model installed in the vein.

Figure 5-8: Model installed in the vein of the wind tunnel.

In the following, we will analyse the aerodynamic torsors and pressure fields. However, the two measurements were not made during the same runs. This is because, to carry out the pressure field measurement, it is necessary to connect the connectors to the scanner, as discussed in sub-chapter 5.1. The scanner must be powered, and simultaneously, it needs the reference pressure employing a vinyl that passes through the vein's underside. This causes an elastic connection between the model and the ground; this aspect does not allow to have correct values of the aerodynamic torsor. To avoid incorrect values, we must decouple the tests for the measurement of the aerodynamic torsors and the tests for the pressure field analysis. An image of the model after the scanner instrumentation is shown in Figure 5-9.

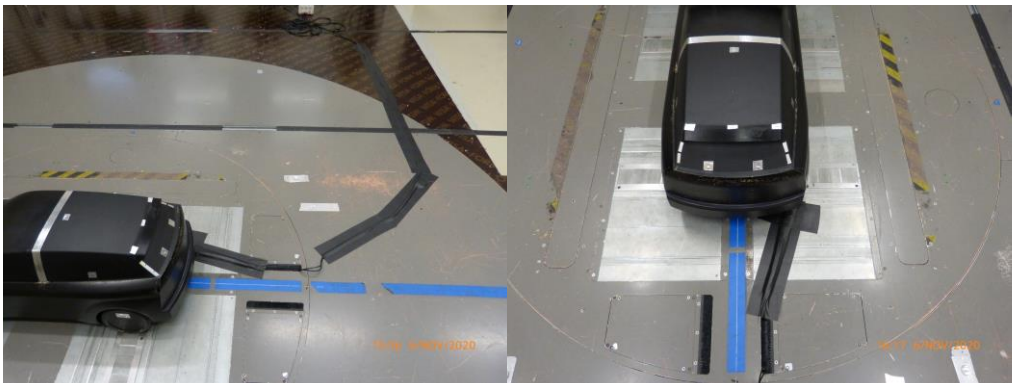

Figure 5-9: Installation and connection of the two scanners for pressure field analysis.

Comparison of the rear cabin in additive manufacturing and the rear cabin in LAB milling: reference configuration

The reference spoiler was first fitted, and we made several runs with strategic speed/yaw configurations. We did this to cross-check and validate the new rear cabin. The Reynolds effect on drag is now being analysed for the configuration *reference spoiler without flap* (Figure 5-10).

Figure 5-10: Initial configuration, rear cabin with reference spoiler without flaps.

We will compare this configuration with the old rear cabin. This comparison allows us to understand how we have worked with the new one's design and production. Subsequently, all tests in speed climbing are carried out with a yaw angle β = 0° while all yawing tests are carried out with V = 50 m/s.

Figure 5-11: Reynolds effect on drag for the two rear cabins, old one in red (Week 28) and new one in blue (Week 45); all values are scaled to the SCx calculated at 50 m/s during W28.

In Figure 5-11 we make a comparison between the two rear cabins with a speed increase (Reynolds climb). Overall, the new cabin has a lower drag compared to the old cab (iso-configuration). Besides, the blue curve has a behaviour, related to the Reynolds effect, which is closer to what is expected, i.e. lower drag for a Reynolds climb.

Now we look at the behaviour in the pressure field. First, a comparison is made between the two cabins at the same speed. The pressure field is then compared for two different speeds on the same cabin (new cabin in additive manufacturing).

Before starting the analysis, it is important to specify that some pressure tappings are not considered because the value obtained was not physical. With certainty, we know that a tapping on the scanner does not work; we do not know if the other values we have obtained are due to a bad installation of the vinyl tubes or other sources of error. To carry out this analysis, we have excluded the points that have a value that is too different from the average field in the surrounding area unless a physical explanation can be brought (continuity of the pressure field). The excluded points do not appear in all the following images. Furthermore, concerning the first analysis (Figure 5-12), the number of pressure tappings is not the same between the two configurations compared. This is due to the change of the cabin. The old model had a lower number of pressure tappings.

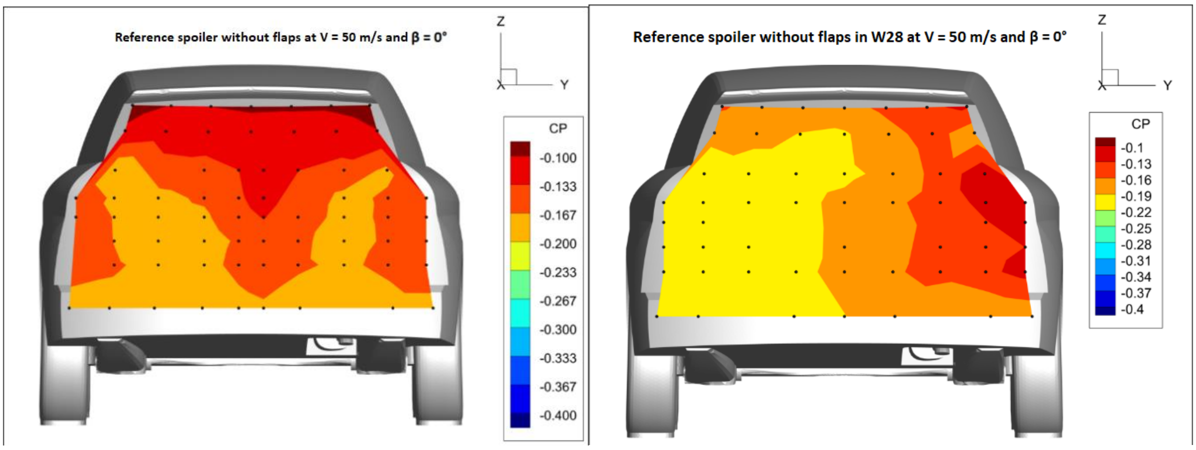

Figure 5-12: Comparison of the pressure field at iso-speed between the configuration Reference spoiler without flaps; V = 50 m/s both for the W45 on the left and for the W28 on the right. ([8]).

Although one might think that the configurations analysed are different, in Figure 5-12 two identical configurations are compared. A slightly asymmetrical wake can be seen on the left-hand side, while a much more pronounced asymmetry is present on the right-hand side. We know that the two pressure fields are obtained respectively during the two sessions, W45 and W28. It is not yet known why there is such a marked difference. Several hypotheses have been made to give an answer to this phenomenon. The model could have a wake subject to static instability, which is still to be proven. Besides, we have a different model, with the rear cabin in additive manufacturing on the left-hand side and the rear cabin in LAB milling on the right-hand side. Besides, the scanner's connection wiring has been placed differently, which could impact the flow. Something could have changed in the wind tunnel itself, so there could be a source of error that we are not aware of. Finally, here we have plotted the average of the C_p measured for one minute, so we could have a highly unsteady wake, which is never equal to its average or whose realisations over the measurement interval are different.

Now the pressure fields at two different speeds with the same cabin are compared. We change the Cp scale and keep it for all the results obtained in W45. The scale used previously, in Figure 5-12, has been used to have results consistent with those obtained by [8].

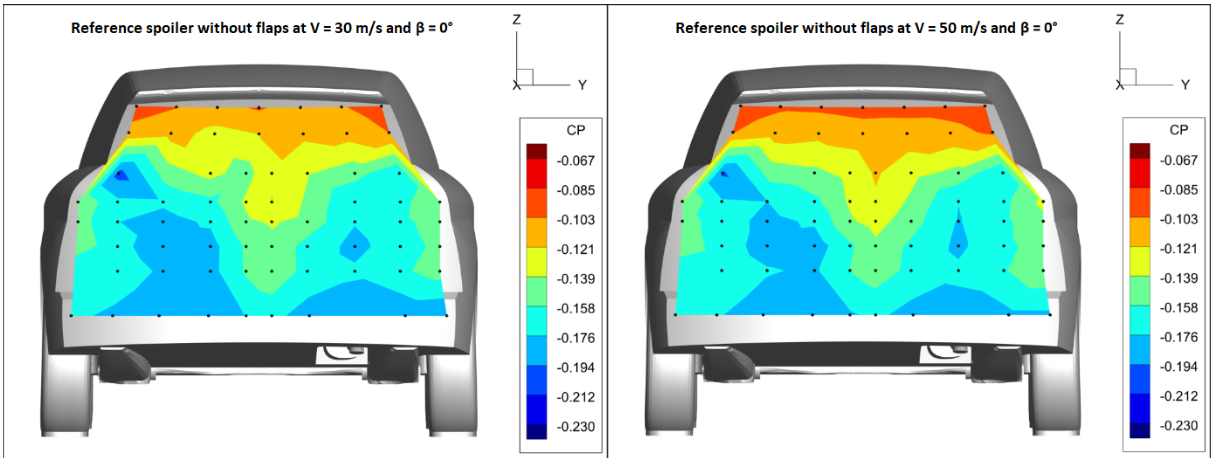

Figure 5-13: Comparison of the pressure field at iso configuration (reference spoiler without flaps) for two different velocities; respectively V = 30 m/s on the left-hand side and V = 50 m/s on the right-hand side.

We can observe that the left/right asymmetry is maintained, which means that in this case, negative yaw angles are needed to symmetrize the wake (Figure 3-6). Overall, we observe that the C_p at the base increases as we increase speed, explaining why we have a smaller SC_x. One might think that the asymmetry is due to the geometric asymmetry of the underbody (Glossary). Still, it is indeed not the only reason, because, with a different rear cabin, fastback type, we observe a significant asymmetry reduction ([8]).

Of course, it is not possible to conclude the new cabin's validity just by analysing the performance during the climbing speed alone; we must also analyse yaw angle effects and flaps influence on the wake.

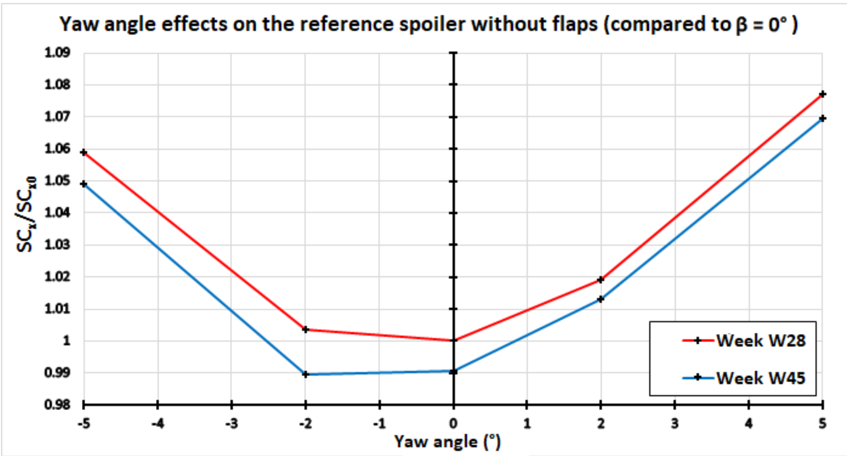

Figure 5-14: Evaluation of the yaw angle effect on drag for the two rear cabins, old cab in red (Week W28) and new cab in blue (Week W45); all values are scaled to the SCx calculated at V = 50 m/s and β = 0° at the W28.

Figure 5-14 shows the yaw angles effect on the two cabins. We can see that the trend is the same. The asymmetry is maintained, but on average, the new cabin has less drag, which is in line with the results shown in Figure 5-11. We cannot conclude whether this is due to an interaction between the rear cabin and the foam model or other factors. Again, we cannot fully validate the new cabin yet. It is essential to understand how it interacts with the flaps.

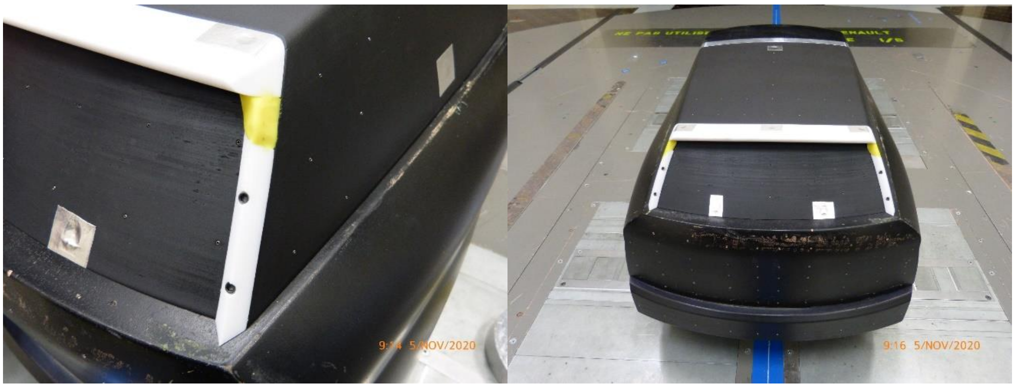

Figure 5-15: Installation of the flaps on the model, sealing with yellow modelling clay to allow the continuity of the flap.

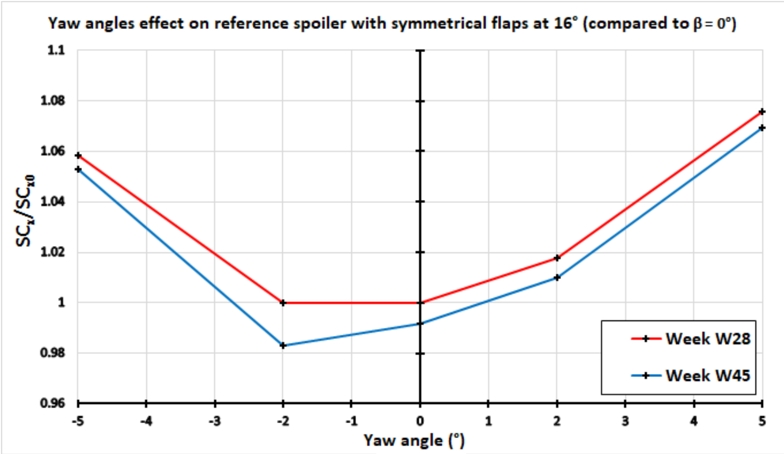

Figure 5-16: Evaluation of the yaw angle effect on drag for a configuration with reference spoiler and symmetrical flaps inclined at 16°; old cabin in red (Week 28) and new cabin in blue (Week 45); all values are scaled to the SCx calculated at β = 0° during S28.

In Figure 5-16 we can see the yaw angles effect on the configuration seen in Figure 5-15. It should be noted that the counterbored holes in the flaps are not plugged and will not be plugged for the other configurations. In fact, it has been verified that the influence of these holes on the aerodynamic torsor is negligible.

The behaviour observed in Figure 5-16 is in line with the results previously obtained. However, here we see that the minimum drag point is around -2° of yaw. The three days of testing and those carried out in week 28, have shown that the model does not produce a symmetrical wake, we have a slight asymmetry of about -1° ([8]). In Figure 5-16, we can see that this aspect seems to be accentuated on the new model. Due to lack of data, it is impossible to know where the minimum drag is on this configuration with the new cabin. Besides, the flaps in week 28 were modelled by hands and therefore had an approximate geometry. For these reasons, we cannot be sure whether the asymmetry is more significant.

The analysis and validation of the cabin is completed by studying the pressure field of this configuration (Figure 5-15).

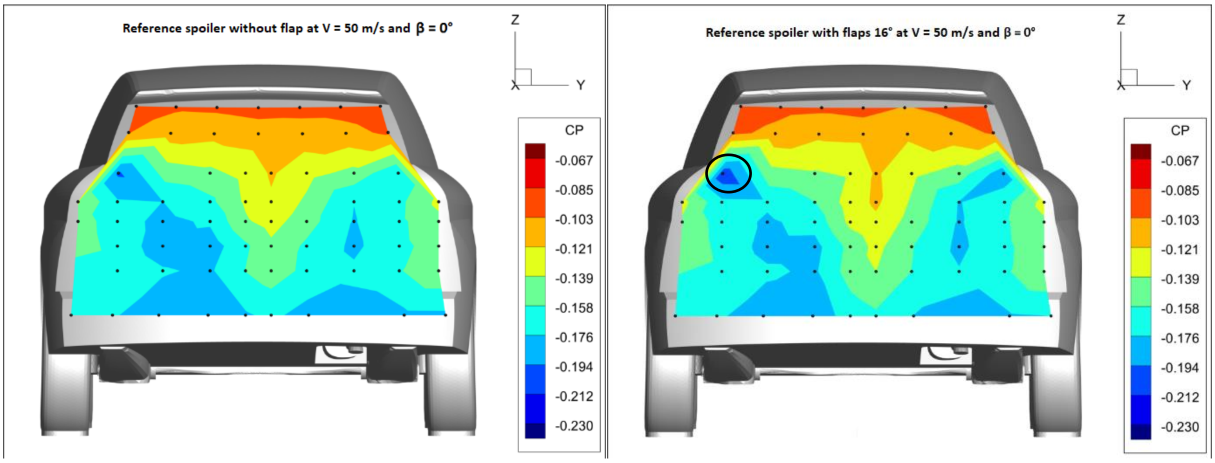

Figure 5-17: Comparison of the pressure field at the base between reference spoiler without flaps and reference spoiler with 16° symmetrical flaps; for both configurations we have V = 50 m/s and β = 0°.

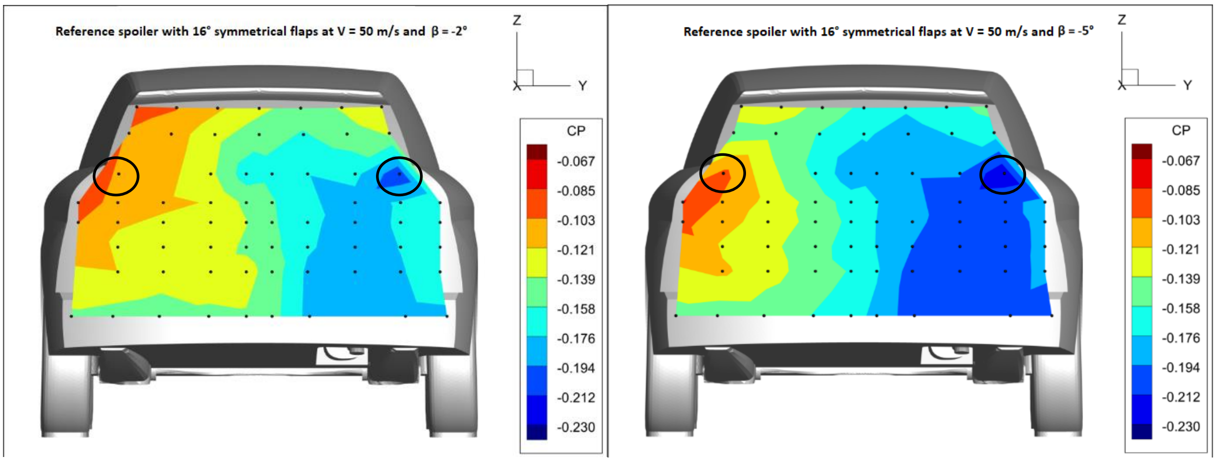

Figure 5-18: Comparison between different yaw angles at iso-configuration (Reference spoiler with 16° symmetrical flaps); left-hand side β = -2° and right-hand side β = -5°, for both V = 50 m/s.

First, Figure 5-17 is analysed. We can see that with the flaps, the pressure field at the base is less asymmetrical. There is an increase in pressure on the two vertical tapping lines in the middle of the base, which is certainly due to the change in the recirculation zone. Besides, an area of low pressure can be seen surrounded in black, which was not present in the configuration without flaps. This is certainly due to an end vortex generated at the corner of the intersection between the flaps and the LAB milling model base. We can be certain of this phenomenon because there is a pressure drop also on the right side; however, it is more emphasised on the left side due to the asymmetry of the flow. Overall, the C_p at the base increases, contributing to the lower value of the SCx in the configuration *reference spoiler with 16° symmetrical flaps*. However, it is essential to analyse the flaps' influence on the yawing vehicle's wake (Figure 5-18).

Because of the yawing, the end vortex effect in the areas surrounded in black is considerably reduced. It is easy to understand that the red/orange area is the windward part (Figure 3-6), where the flap has a significant influence ([1]). The aerodynamic torsor results show a significant gain; however, the yawing pressure field for the configuration reference spoiler without flaps is not available. For this reason, it is not possible to draw any quantitative conclusions about the influence of the flaps on the pressure field. The pressure field is not shown for the positive angles, as the geometry is symmetrical and therefore it would be like that shown in Figure 5-18.

For the results observed, we can consider ourselves satisfied. The cabin is validated, and the analysis of the EVO spoiler will now be carried out.

Evaluation of the EVO Spoiler and its interaction with flaps

The EVO spoiler has been designed with rules given by the aerodynamic department. Therefore, it is expected to see an improvement in terms of drag. The next studied configuration is shown in Figure 5-19.

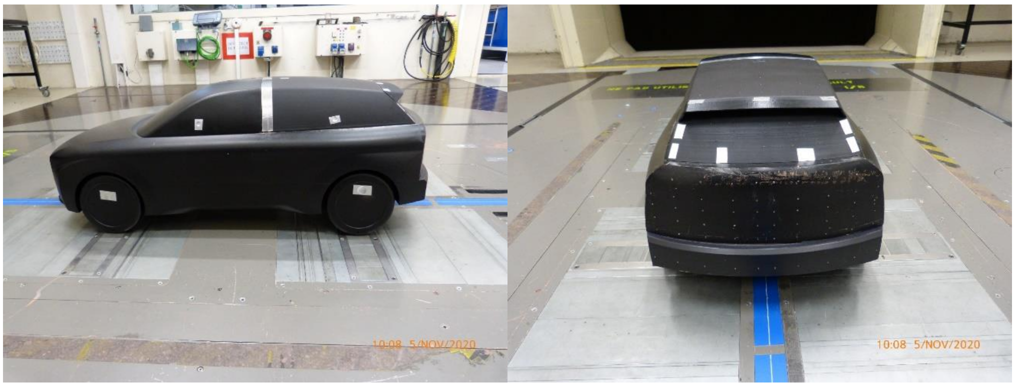

Figure 5-19: EVO spoiler installed on the rear cabin.

First, we want to see its behaviour according to speed increase, so we evaluate Reynolds effect.

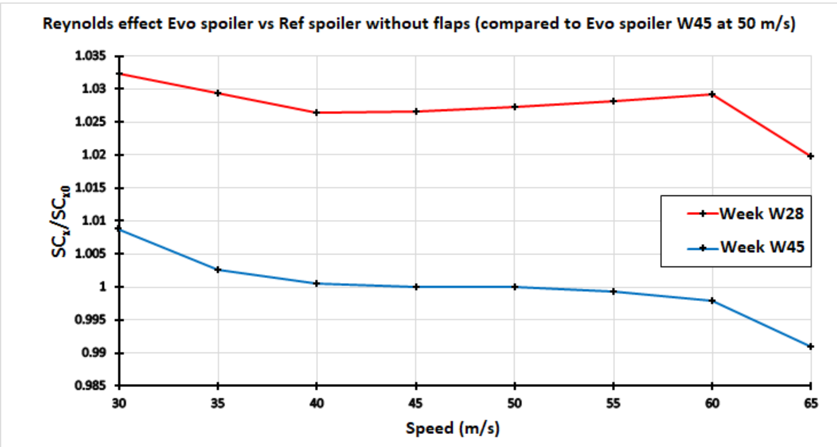

Figure 5-20: Reynolds effect on drag for EVO Spoiler, configuration Reference spoiler W28 in red and configuration EVO Spoiler W45 in blue; all values are scaled to the SCx calculated on the EVO Spoiler at 50 m/s and β = 0° during W45.

We chose to compare the *EVO Spoiler in week 45* with the *Reference spoiler in week 28* because for the *reference spoiler in week 45* there are not enough points available for a detailed analysis (Figure 5-11). We can observe that the behaviour is close to our expectations: the SC_x always decreases as the Reynolds increases. Overall, we can see an improvement of around 3% over the entire speed range, which confirms that the EVO spoiler does indeed provide a significant gain in terms of aerodynamic torsor.

The gain brought should also be visible in terms of increase of Cp at the base. For this reason, the pressure field for the configuration *EVO Spoiler without flaps,* and its stake in relation to the configuration *reference Spoiler without flaps,* is analysed in Figure 5-21.

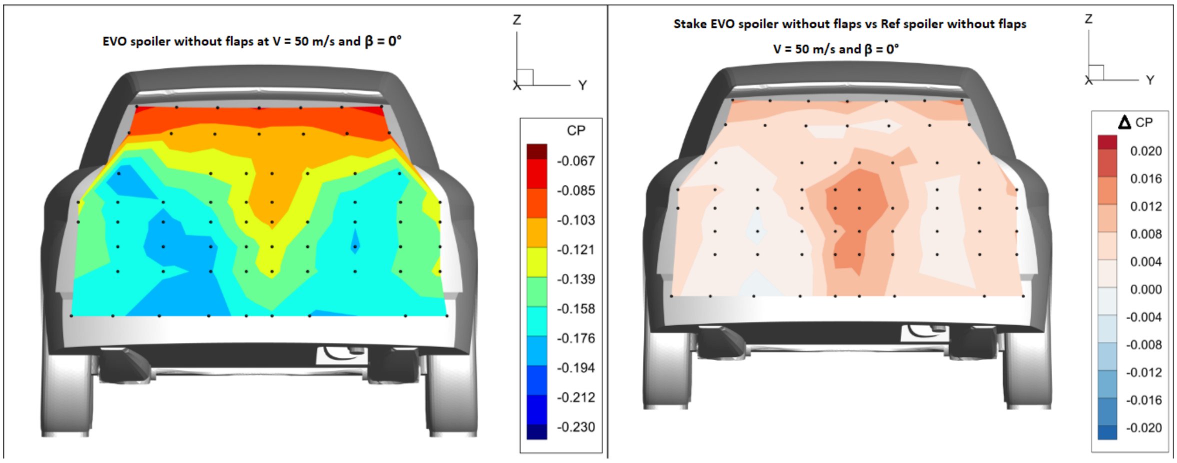

Figure 5-21: On the left-hand side the pressure field for the configuration EVO Spoiler without flaps, on the right-hand side the stake between EVO Spoiler without flaps and Reference Spoiler without flaps; for both images we have V = 50 m/s and β = 0°.

Overall, the C_p is increasing, which explains the decrease in SC_x. However, we can observe that the pressure does not increase steadily. The left/right asymmetry is maintained. Moreover, using the image on the right side of Figure 5-21, one could think that it is even increased. The recirculating torus, structure 2 Figure 3-2, is undoubtedly modified. This explains the different pressure field in the central part of the base. However, we cannot conclude on the end vortices with the data available.

However, consideration must also be given to whether the gain is maintained while yawing, because, as already explained in Chapter 3, the yaw angle is different from 0° about 90% of the time under real conditions.

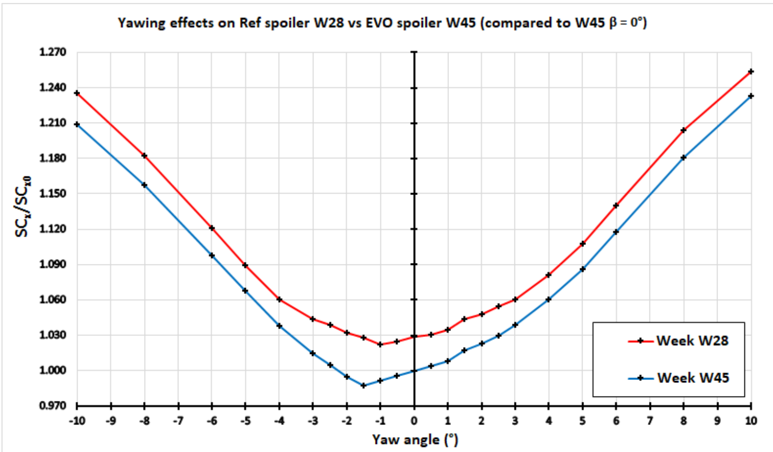

Figure 5-22: Yawing effects on drag for the configuration EVO Spoiler without flaps; in red Reference Spoiler without flaps W28 and in blue EVO Spoiler without flaps W45; all values are scaled to the SCx calculated on the EVO Spoiler at β = 0° during W45

Here again, we have chosen to compare the configuration *EVO Spoiler in week 45* with the *Reference spoiler in week 28* to have consistency in terms of the points analysed. In Figure 5-22, we can see that the trend is always similar. The left/right asymmetry mentioned earlier is still present. Due to a lack of data, it is impossible to know whether the EVO Spoiler also influenced the asymmetry or not, as we cannot compare it with the configuration *reference Spoiler in week 45*. It cannot be concluded to what extent the spoilers influence the asymmetry. What is known from [8] is that with a different rear cabin (fastback without massive flow separation), the asymmetry disappears. We could obtain more details from the pressure field analysis; however, it was impossible to measure the C_p for the configuration

EVO Spoiler without flaps in yawing conditions due to lack of time. The only thing that can be stated with certainty is that the asymmetry is still present even with the new rear cabin and the EVO spoiler.

Overall, we can see that the stake between the *EVO Spoiler without flaps* and the *reference Spoiler without flaps*, in terms of drag, becomes smaller as the yaw angle increases. This means that there is a more significant degradation with the EVO spoiler depending on the yaw angle. This is also confirmed by the values in Table 1.

β (°)	ΔSCx
-5°	-1.09%
-2°	-2.27%
0°	-1.87%
2°	-1.85%
5°	-1.34%

Table 1: Stake in terms of SCx between EVO Spoiler without flaps in W45 and Reference Spoiler without flaps in W45 at different yaw angles; for both configurations V = 50 m/s; values in green, beneficial stake; values in red, disadvantageous stake.

To complete the analysis, the two spoilers on the same cabin were also compared. We can see that the gain, in terms of drag, is indeed quite significant. The trend shown in Figure 5-22 is still present, the EVO Spoiler is less effective for large yaw angles, although it still provides beneficial effects. As a result, there is a more significant degradation as a function of the yaw angle.

Now we need to analyse the flaps effect and the interaction with the EVO Spoiler. It is known that for the rear cabin in LAB milling, the 16° flap inclination represents the best configuration of those tested. Since both the spoiler and the cabin has been changed, we cannot be sure that the best configuration is always the same. For these reasons, we tested all flap inclinations.

Only one flap, specifically the left one, was used to establish the best configuration. This is because, in the case of adaptive automobile aerodynamics, one could consider hiding the flap leeward, for example, with a 90° inclination (Glossary). This aspect is crucial because we have seen, thanks to [8], that an asymmetrical windward flap provides more beneficial effects compared to a configuration with symmetrical flaps. Figure 5-23 shows an example of a left asymmetrical flap configuration.

Figure 5-23: Configuration with EVO spoiler and asymmetrical left flap inclined at 16°.

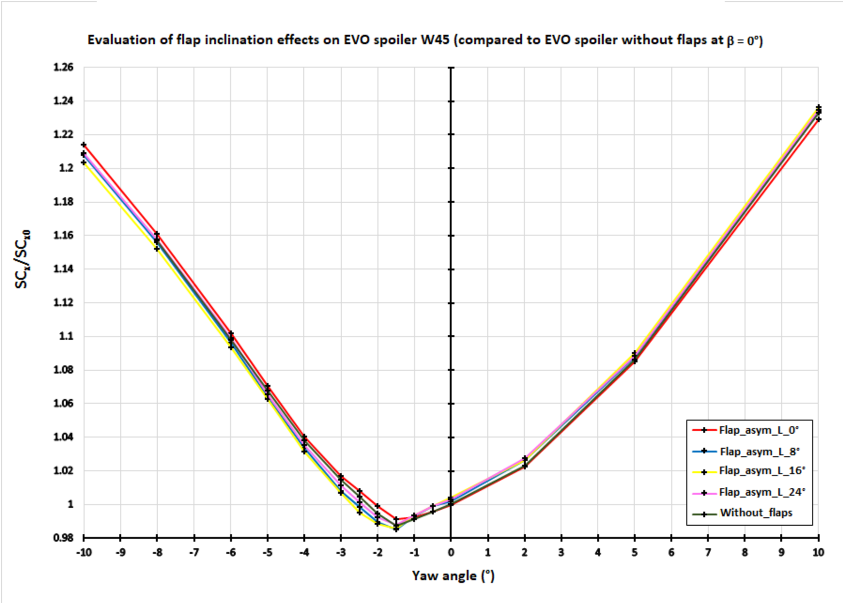

Figure 5-24: Analysis of the yawing effect on drag for all flap inclinations in interaction with the EVO Spoiler; all values are scaled to the SCx calculated on the EVO Spoiler without flaps at β = 0° during W45.

It can be seen in Figure 5-24 that the trend is very similar for all flap configurations. In fact, the curves almost overlap. The biggest difference is observed with windward flaps (Figure 3-6). It is important to note that the results are like those obtained with very simplified geometries such as Ahmed's body. [1].

To see which configuration is the best, we must consider the overall trend. Still, as in this case we have very similar tendencies we preferred to focus on an area of interest. In this case, we have chosen yaw angles between -3° and 0°, which are angles where the left flap is windward and therefore brings more significant beneficial effects.

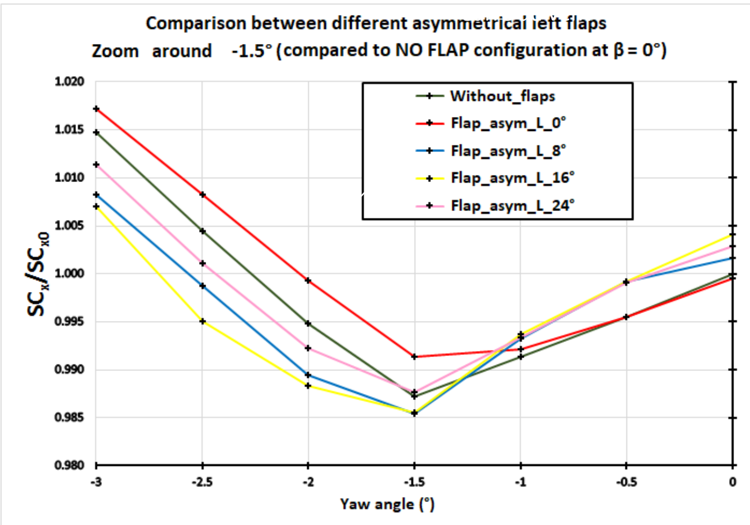

Figure 5-25: Enlargement of Figure 5-24 between -3° and 0° to evaluate the best flap configuration; all values are scaled to the SCx calculated on the EVO Spoiler without flaps at β = 0° during W45.

We can see that we have the maximum gain with the flap inclined at 16°. For this reason, we consider the 16° inclined flap as the best flap configuration for our study. Besides, we also analysed the pressure field associated with this configuration.

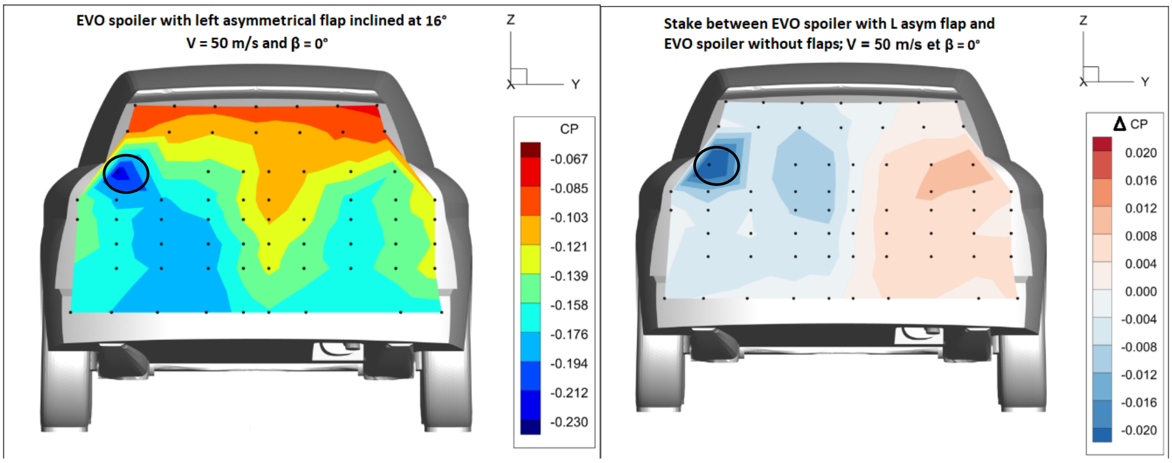

Figure 5-26: On the left-hand side the pressure field for the configuration EVO Spoiler with left asymmetrical flap at β = 0° and V = 50 m/s; on the right-hand side the stake between EVO Spoiler with left asymmetrical flap and EVO Spoiler without flaps at β = 0° and V = 50 m/s.

Overall, in Figure 5-26, we see an increase in C_p on the right side of the base, while on the left side, there is a decrease in C_p with a very marked end vortex. This aspect is in line with what has been observed in terms of SC_x. In fact, for zero-yaw, the left asymmetrical flap inclined at 16° does not bring any beneficial effects. The flap's presence increases the end vortex's power generated in the corner between the flap and the LAB milling model. As expected, given the asymmetrical geometry, an asymmetry has been added due to the flap's presence only on the left. The increase in C_p on the base's right side is undoubtedly due to the different interaction that occurs when the flap is present. Therefore, we can state that the recirculation bubble has been modified.

However, it is interesting to see how the left asymmetrical flap modifies the pressure field in yawing, where we can see a beneficial effect.

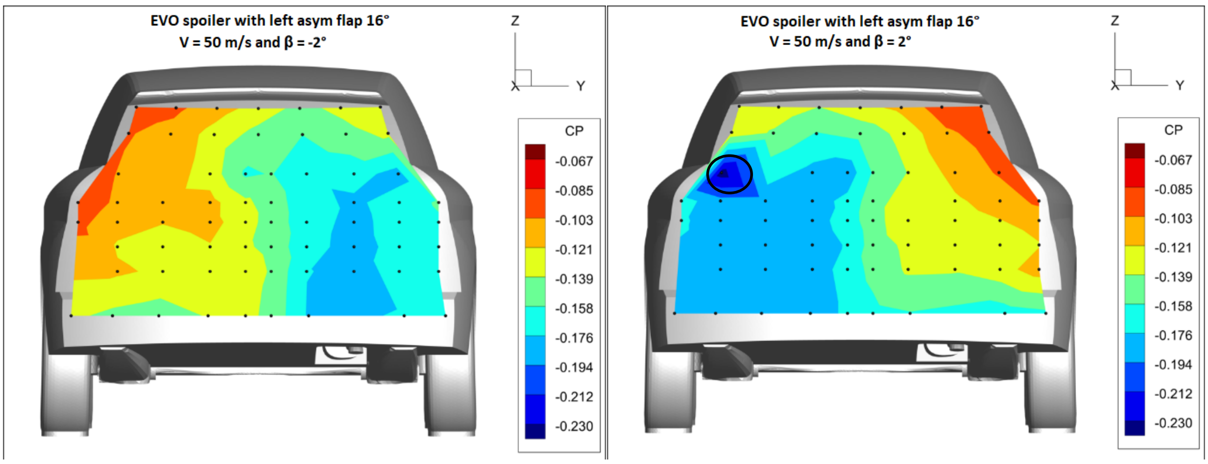

Figure 5-27: Comparison between different yaw angles on the same configuration EVO spoiler with 16° left asymmetrical flap; β = -2° on the left-hand side and β = 2° on the right-hand side, for both V = 50 m/s.

We will analyse only β = ± 2° in Figure 5-27. This is because the trend is similar, but more marked, in the case β = ± 5°. Overall, we can see that the effect of the windward flap is beneficial. A higher-pressure part characterises the vehicle's windward side, but this area is even larger with the flap's presence. If we now look at the vehicle's leeward side, we see a large area with low pressure, which becomes smaller when the edge is present. Besides, as there is no leeward flap for β = -2°, the right end vortex is not present, an aspect which contributes to the overall increase in C_p. However, we can see the inefficiency of the flap as soon as it is leeward. It contributes to the generation of the left-hand end vortex, which increases drag. This also explains the non-beneficial results observed in terms of SC_x when the flap is leeward.

Therefore, the configuration with a 16° inclined flap is validated as the best configuration. Hereafter, we will analyse the right asymmetrical flap behaviour inclined at 16° and that of the symmetrical configuration.

Figure 5-28: On the left-hand side the configuration EVO spoiler with right asymmetrical flap inclined at 16°; on the right-hand side the configuration EVO spoiler with symmetrical flaps inclined at 16°.

For a direct comparison, the three different configurations are plotted on the same graph. The result is shown in Figure 5-29.

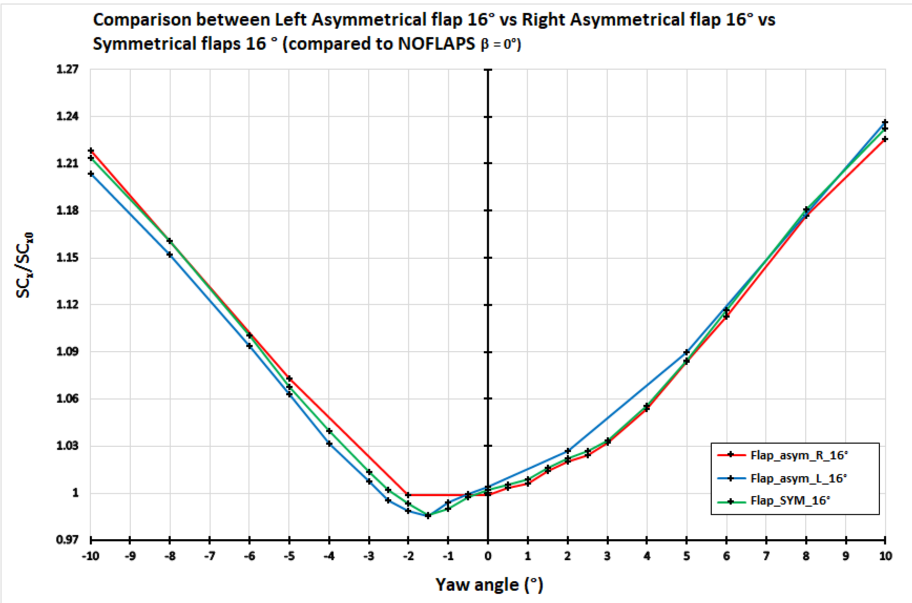

Figure 5-29: Yawing effect on drag for the configuration with symmetrical flaps and both configurations with an asymmetrical left and right flap respectively; all values are scaled to the SCx calculated on the EVO Spoiler without flaps at β = 0°.

Figure 5-29 shows the same trend as observed previously. Asymmetrical flaps provide more significant gains as soon as they are windward, whereas for small yaw angles (between -1.5° and 0°) the symmetrical configuration is better, in terms of drag. Globally, we have a gain of around 1% compared to the configuration without flaps which could seem small but is important.

However, there is also an important aspect to consider. If we look at the effect of the flaps in both cases, i.e. when coupled with both spoilers, we can see that the gain is smaller with the EVO spoiler. This leads us to believe that, if the flaps are placed on already optimised models, they provide less beneficial effects.

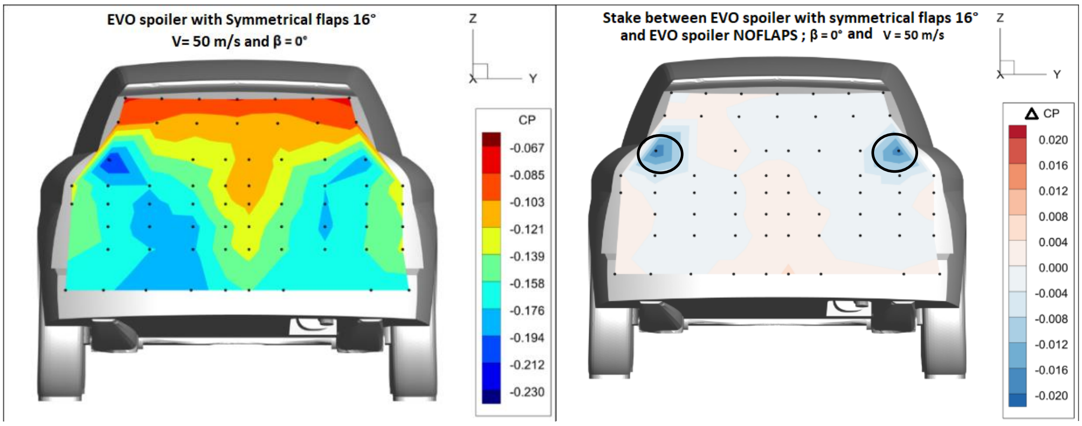

Figure 5-30: On the left-hand side the pressure field of the configuration EVO Spoiler with 16° symmetrical flaps; on the right-hand side the difference between this configuration and the configuration EVO Spoiler without flaps; for both images V = 50 m/s and β = 0°.

Hereafter, the effect on the pressure field of the configuration with symmetrical flaps is evaluated. Once again, the intensity of the end vortices is increased with the presence of the flaps; this characteristic can also be seen on the right-hand side of Figure 5-30. In terms of SC_x, no change is observed, which is not obvious when looking at the stakes (right part of Figure 5-30). The interaction between the EVO Spoiler and the 16° inclined flaps does not seem to produce beneficial effects for a zero-yaw angle. For this reason, one might think that there is no point in having symmetrical flaps for β = 0°. However, it must be considered that there is a limited database and therefore no conclusion can be drawn on this aspect. We now analyse the effects of the yawing on the pressure field.

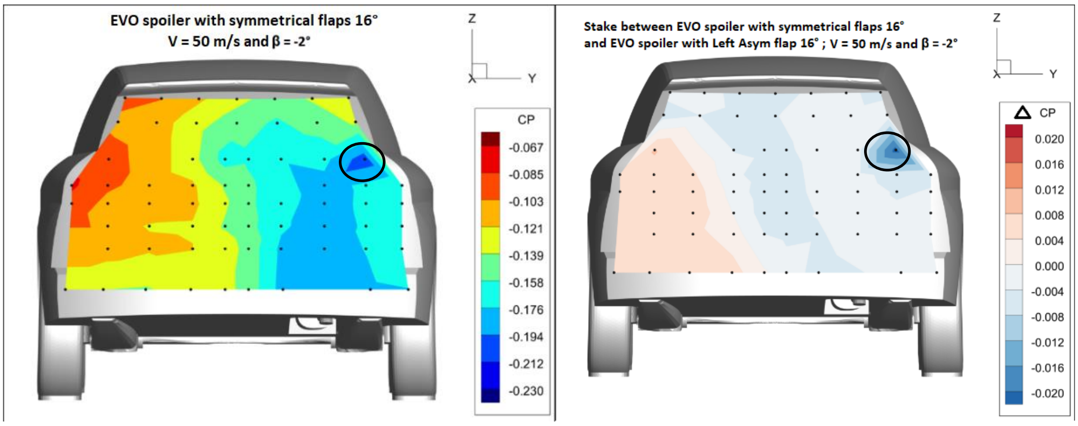

Figure 5-31: On the left-hand side the pressure field of the configuration EVO Spoiler with 16° symmetrical flaps; on the right-hand side the stake between this configuration and the configuration EVO Spoiler with 16° Left Asym flap; for both images V = 50 m/s and β = -2°.

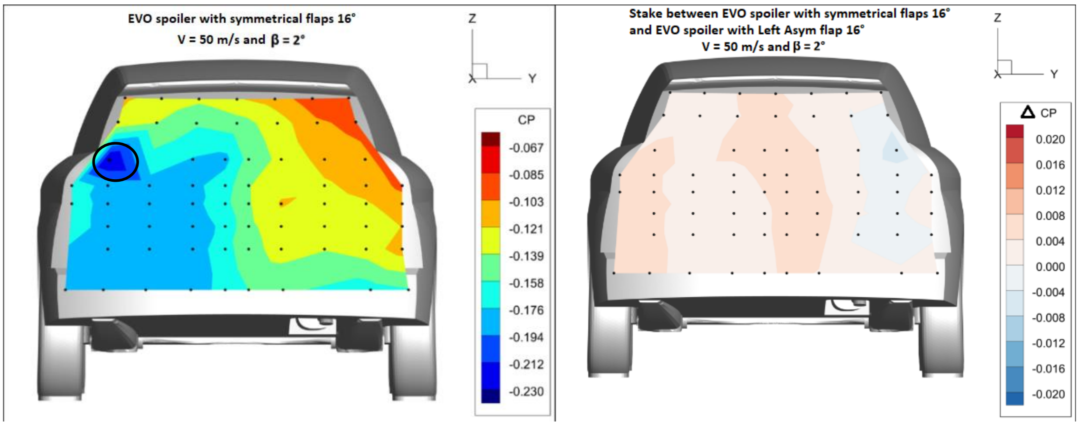

Figure 5-32: On the left-hand side the pressure field of the configuration EVO Spoiler with 16° symmetrical flaps; on the right-hand side the stake between this configuration and the configuration EVO Spoiler with 16° Left Asym flap; for both images V = 50 m/s and β = 2°.

In this case, we will also analyse only β = ± 2°, in Figure 5-31 and Figure 5-32, for the same reason detailed above. The results are in line with those observed so far. It can be observed that for negative yaw angles, i.e. left windward flap (Figure 3-6), the configuration with symmetrical flaps increases the C_p at the base. However, if we consider the configuration with the asymmetrical left flap and calculate the stakes, it is possible to observe that the C_p decreases on average. This is in line with the results in terms of SC_x: the asymmetrical flap windward brings a more significant gain compared to the configuration with symmetrical flaps.

If we consider positive angles, right flap windward (Figure 3-6), we can underline the importance of having a windward flap. We can observe a significant improvement for positive angles if we compare the configuration *Symmetrical Flaps 16°* to the configuration *Left Asymmetrical Flap 16°*. This yields an unexpected but crucial result: having a windward flap is important.

These results are in line with our analysis also carried out on the SC_x. Indeed, we observe that having a strategy to control flap inclination could be interesting to always have an optimal gain. Furthermore, this behaviour, as well as the results shown by [1], leads us to believe that configurations with two asymmetric flaps, simultaneously, could provide a more significant gain. For this reason, we thought of testing two different configurations, the first is a configuration with a right flap at 16° and a left flap at 0°, while the second is the opposite, i.e. a left flap at 16° and a right flap at 0°.

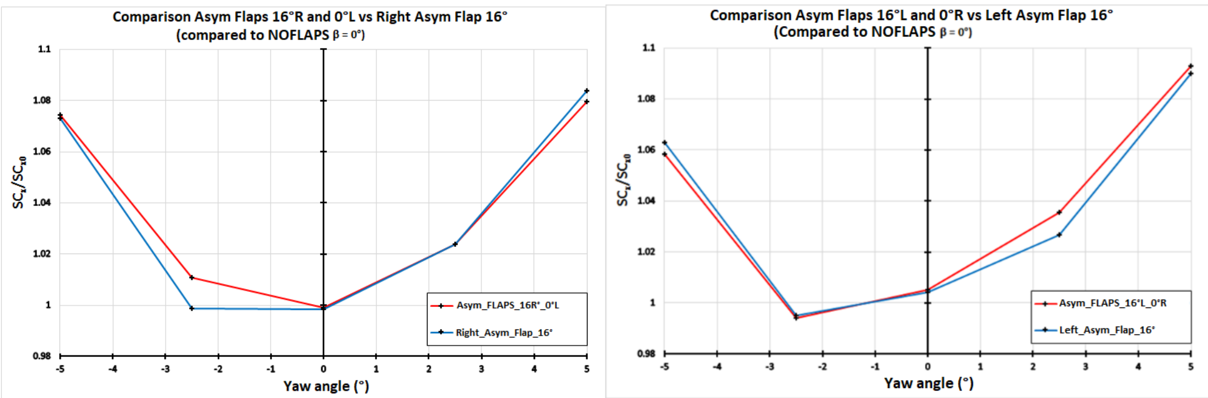

Figure 5-33: Yawing effect on drag for two different configurations; left-hand side EVO Spoiler with asymmetrical flaps 16°Right and 0°Left; right-hand side EVO Spoiler with asymmetrical flaps 16°Left and 0°Right.

The results shown in Figure 5-33 are auspicious. If the most inclined flap in the two-sided asymmetrical configuration is windward, a slightly more significant gain is achieved compared to the single-sided asymmetrical configuration. Of course, we cannot yet draw precise conclusions, as only few values have been measured, and only one configuration with two asymmetrical flaps has been tested. However, this allows us to say that we have very similar results to [1] even with a much more complex model. Of course, it is possible to continue to study different configurations with two asymmetrical flaps. We can even carry out a more detailed characterisation with a wider range of yaw angle values.

β (°)	ΔSCx	ΔSCx
-5°	0.15%	-0.45%
-2°	1.22%	-0.10%
0°	0.04%	0.11%
2°	-0.00%	0.89%
5°	-0.42%	0.30%

Table 2: Stake, in terms of SCx, between 4 different yawing configurations; in the left part we compare the configuration with two asymmetrical flaps 16°R 0°L and the configuration Right Asym flap 16°; in the right part we compare the configuration with two asymmetrical flaps 16°L 0°R and the Left Asym flap 16° ; for all configurations V = 50 m/s; values in green, beneficial stake; values in red, penalizing stake.

In Table 2, numerical values have been reported to further detail the analysis of asymmetrical flaps configurations. A gain is indeed seen as soon as the flap the most inclined is windward. Moreover, a similarity can be observed for both cases. When the most inclined flap is windward, we see similar gains. However, there is a behaviour that cannot be explained yet; if the least inclined flap is windward, there are penalizing effects. This is most likely due to the interaction of the flow with the most inclined flap, which in this case is leeward. Due to lack of time, it has not been possible to carry out a pressure field analysis on these two configurations, so it is interesting to go further in the future. It is also important to study several asymmetrical configurations to see the influence between the two flaps.

So far, the gain in terms of SC_x has been considered. However, it should not be forgotten that a gain in SC_x could bring a degradation of the SC_{zar} (Figure 5-7).

β (°)	ΔSCzar
-5°	2.28%
-2°	2.63%
0°	2.14%
2°	2.66%
5°	1.84%

Table 3: Yawing effect on stake in terms of SCzar for EVO Spoiler with 16° symmetrical flaps and Reference Spoiler with 16° symmetrical flaps; values in green, beneficial stake; values in red, penalizing stake.

The SC_{zar} shows us how much lift we have on the rear axle of the car. In our case, we do indeed have a degradation of the SC_{zar}. However, the values obtained fall within the range of values that are acceptable for the company. We accept to degrade the SC_{zar} to a certain extent if the contribution in terms of SC_x is interesting, which is indeed shown in the results analysed previously.

The same consideration is to be made with the SC_n, a coefficient that refers to the stability of the vehicle. To analyse this coefficient a very large yaw angle is imposed, i.e. $\beta = \pm 30°$.

β (°)	ΔSCn
-30°	-0.27%
30°	0.30%

Table 4: Effect of configurations on vehicle stability, stake in terms of SCn for the configuration EVO Spoiler with 16° symmetrical flaps and the configuration Reference Spoiler with 16° symmetrical flaps; for both configurations V = 40 m/s; values in green, beneficial stake; values in red, penalizing stake.

In this case, SC_n degradation is also observed, however the degradation is low and therefore negligible compared to the significant gains made by the EVO spoiler and flaps in terms of SC_x.

5.3. Synthesis of the results

The new rear cabin in additive manufacturing shows similar results to the old LAB milling cabin, in terms of aerodynamic torsor. However, the base's pressure field is very different: the old cabin has a strong wake asymmetry, which is reduced in the new one. As of now, it is unknown whether this is due to instability in the model's wake or whether the old rear cabin had an unexpectedly large asymmetry in geometry or whether the asymmetry comes from the wind tunnel itself.

Once we validated the new cabin, a new spoiler was tested. The latter follows the rules imposed by the PSA Group's aerodynamics department. This spoiler is optimised; it presents very interesting results both in terms of aerodynamic torsor and pressure field. On average, a gain in terms of SC_x of around 1% can be observed. This gain is also explained by the increase in C_p at the base. However, even if it still shows a gain compared to the old reference spoiler, it has a more significant SC_x degradation, depending on yaw angles. Hence, the sensitivity to yawing is increased. Besides, we should not forget the behaviour in terms of SC_{zar} and SC_n. In our case, we observe a slight degradation for these two coefficients. However, this degradation is negligible compared to the gains made by the EVO spoiler and the flaps in terms of SC_x.

The initial idea, linked to my internship subject, and therefore to the adaptive automobile aerodynamics, is to validate certain aerodynamic devices' effectiveness. These devices can move by adapting to the environment's conditions around the vehicle. Being a preliminary analysis, we imagined testing the flaps in static configurations with different inclinations in a variable yawing flow.

The results obtained with the coupling of the reference spoiler and the flaps are auspicious. The gain obtained with the coupling between the EVO spoiler and the flaps is even better. However, in the latter case, the flap has less influence, because the optimized spoiler leads to a wake generating less drag so there is less to gain. The optimisation of the spoiler, coupled with the flap's presence, shows an increase in the end vortex intensity, generated in the corner between the flap tip and the upper part of the LAB milling model (circled in black in Figure 5-30).

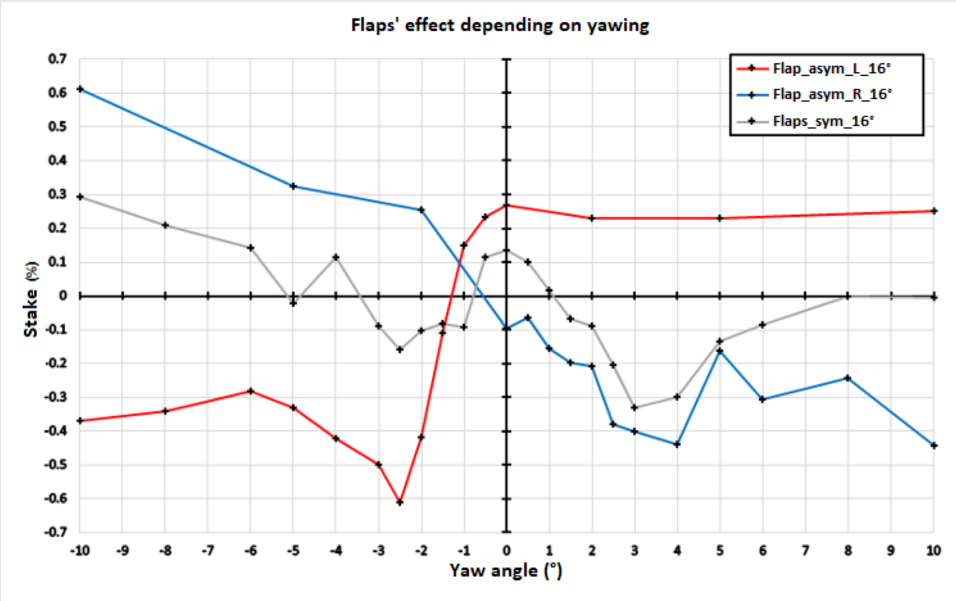

Figure 5-34: Flaps' effect depending on yawing; the zero line is referring to the Evo spoiler without flaps.

Simultaneously, the importance of having a windward flap was also stressed, as also underlined in Figure 5-34. Whenever we have an asymmetrical windward flap, the gain is important. The same flap, when it is leeward, does provide penalizing effects though. The configuration *symmetrical flaps* appear to be the best one only for little negative angles. However, we found that an asymmetrical coupling of the flaps could be an exciting solution (Figure 5-33). This leads us to believe that it might be possible, for future trials, to try several asymmetrical flaps configurations to get a clearer idea of this phenomenon. These tests would be interesting in the optic of adaptive automotive aerodynamics, in fact the optimal trend is always advantageous, as shown in Figure 5-35 where we simulate flaps adapting to the yaw angle.

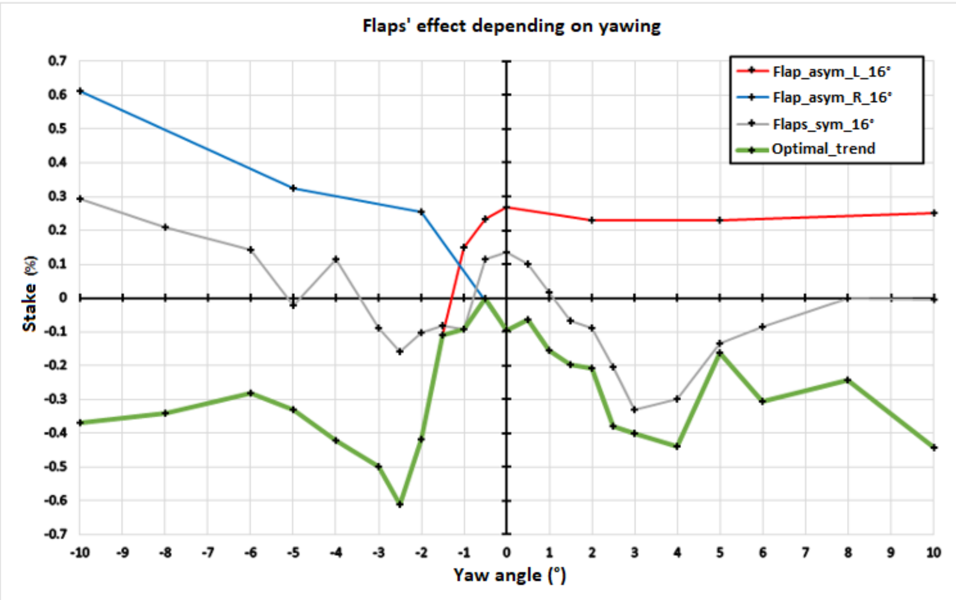

Figure 5-35: Optimal trend simulating moving flaps adapting to the vehicle's yaw angle.

Besides, it is crucial to understand the unsteady effects present in the atmospheric boundary layer to obtain feedback so that we can adapt control laws to the studied devices.

Configuration	Weighted stakes
Symmetrical flaps	**0.10%**
Left Asymmetrical flap	**0.11%**
Right asymmetrical flap	**0.13%**
Optimal trend	**0.44%**

Table 5: Weighted stakes, according to the wind probability distribution, of the different flap configurations; values in green, beneficial stake; values in red, penalizing stake.

In terms of numerical values, a gain of more than 0.4% has been observed for the optimal solutions. This might seem low; however, we must think that the PSA Group starts investing in aerodynamic projects once the 0.3% mark is crossed.

Overall, the results obtained during the tests are very satisfactory and very useful for future studies. These results have allowed us to answer many questions and ask ourselves others, which we hope to answer in the coming months/years.

6. Conclusions

This End-of-Studies Work allowed us to tackle a very particular subject that is not yet mastered at the current state, i.e. adaptive automobile aerodynamics.

The studies carried out during this internship were very useful and allowed us to understand that vehicle aerodynamics that adapts to the environment, i.e. to the possible speed/yaw configuration, is indeed a viable solution. Preliminary investigations have opened a wide field of questions; the flow around a car is far from obvious, and it is also quite different compared to Ahmed's or Windsor's academic body type configurations. Very often, car wakes are characterised by highly unstable behaviour at non-zero yaw angles. This makes it even more challenging to predict its behaviour and adapt to it. During this end-of-study work it was possible to start building a database that could help the doctoral thesis "Active reduction of aerodynamic drag under operating conditions" that will begin this year. During this doctoral thesis, it will be necessary to continue improving the database as well as to carry out road tests to get feedback on the characteristic flows of the atmospheric boundary layer and their influence on the flow behaviour around the vehicle. With the feedback, consideration could be given to designing a control strategy to reduce drag, which allows the vehicle's aerodynamic devices to adapt to the surrounding environment. However, today we cannot say which is the best strategy to adopt, nor even if there is indeed a strategy that can bring a real gain from an industrial point of view, in terms of reproducibility and costs.

From a personal point of view, this internship has had its ups and downs. Because of the Covid-19, I did most of the work in smart working. This aspect did not allow me to get to know the life of a company entirely. However, despite the health crisis, I was able to carry out and pilot tests in the wind tunnel. I was also able to instrument the models, organise test programmes, post-process test data, etc. All this helped me understand the amount of work that goes into a wind tunnel test. Besides, I learned the rigour required for each part of the work and the importance of optimising the programme for a test session to avoid wasting time and money.

This internship, mainly experimental, allowed me to know aspects of aerodynamics, which were previously only theoretical notions for me. Moreover, the flows around a vehicle are much more complicated than the academic cases studied. Therefore, I was able to work in an environment that I have been passionate about since I was very young. This aspect has been fundamental in helping me understand how passionate I am about this field of study. I have learned to put all the results into discussion, because its complexity does not allow to draw any conclusions at the first approach to the case of study. I have also understood that research, linked to industrial constraints, is something to which I want to devote myself.

To conclude, during these 6 months, I have grown personally and professionally. This experience has given me the opportunity to understand the strong intrinsic link between research and industry, allowing me to understand that this is the path I need to follow to be happy!

Bibliography

[1] J. Garcia de la Cruz, R. Brackston et J. Morrison, «Adaptive Base-Flaps Under Variable Cross-Wind,» *SAE Technical Papers,* 2017.

[2] L. Thomann, «Mesures aérodynamiques en environnement réel,» Rapport de stage, document interne PSA, 2018.

[3] Commission Européenne, «Emissions in the automotive sector,» [En ligne]. Available: https://ec.europa.eu/growth/sectors/automotive/environment-protection/emissions_en. [Accès le 13 10 2020].

[4] L. Point, «Consommations de carburant pourquoi elles sont fausses,» [En ligne]. Available: https://www.lepoint.fr/automobile/innovations/consommations-de-carburant-pourquoi-elles-sont-fausses-18-10-2012-1518257_652.php. [Accès le 13 10 2020].

[5] Y. Goraguer, «Aérodynamique en situations réelles de conduite,» Document interne PSA, 2017.

[6] Commission Européenne, «Réglement parcours Real Driving Emission,» Journal officiel de l'Union européenne, 2016.

[7] Citroën, «NORME WLTP : NOUVELLES HOMOLOGATIONS DES VÉHICULES,» [En ligne]. Available: https://www.citroen.fr/univers-citroen/technologie/homologations-des-vehicules.html. [Accès le 13 10 2020].

[8] C. Melin, «Aérodynamique automobile adaptative,» Rapport de stage - Document interne PSA, 2020.

[9] G. Bonnavion, O. Cadot, V. Herbert, A. Évrard, S. Parpais, R. Vigneron et J. Délery, «On multistabilities of real car's wake,» *Journal of Wind Engineering and Industrial Aerodynamics,* vol. 164, n° %10167-6105, pp. 22-33, 2017.

[10] P. Waudby-Smith, T. Bender et R. Vigneron, «The GIE S2A Full-Scale Aero-acoustic Wind Tunnel,» *SAE International,* n° %12004-01-0808, 2004.

[11] G. Bonnavion, «Dynamics of the unstable wake modes in automotive,» Thèse de doctorat de l'Université Paris-Saclay 2018SACLY010, 2018.

[12] J.-F. Beaudoin et J.-L. Aider, «Drag and lift reduction of a 3D bluff body using flaps,» *Experiments in Fluids,* vol. 491, n° %144, 2008.

[13] O. Cadot, A. Courbois, D. Ricot, T. Ruiz, F. Harambat, V. Herbert, R. Vigneron et J. Délery, «Characterizations of force and pressure fluctuations on real vehicles,» *International Journal of Engineering Systems Modelling and Simulation,* n° %1125051442, 2016.

[14] R. Li, J. Borée, B. R. Noack, L. Cordier et F. Harambat, «Drag reduction mechanisms of a car model at moderate yaw by bi-frequency forcing,» *PHYSICAL REVIEW FLUIDS,* n° %1034604, 2019.

[15] J. Tian, Y. Zhang, H. Zhu et H. Xiao, «Aerodynamic drag reduction and flow control of Ahmed body with flaps,» *Advances in Mechanical Engineering,* vol. 9, n° %17, p. 1–17, 2017.

[16] A. Raina et A. Khajuria, «Assessment of Flow Control using Passive Devices around Bluff Bodies,» *International Journal for Research in Applied Sciences and Biotechnology,* vol. 5, n° %11, pp. 1-5, 2018.

[17] B. Khalighi, S. Zhang, C. Koromilas, S. R. Balkanyi, L. P. Bernal, G. Iaccarino et P. Moin, «Experimental and Computational Study of Unsteady Wake Flow behind a Bluff Body with a Drag Reduction Device,» *Society of Automotive Engineers,* n° %1207, 2001.

[18] M. Varney, M. Passmore et A. Gaylard, «Parametric Study of Asymmetric Side Tapering in Constant Cross Wind Conditions,» *SAE International Journal of Passenger Cars - Mechanical Systems,* vol. 11, n° %13, 2018.

[19] G. S2A, «Mesure de pression en soufflerie,» Document interne GIE S2A, 2015.

[20] Scanivalve. [En ligne]. Available: http://scanivalve.com/. [Accès le 25 11 2020].

[21] G. Hulin, «Pesées aérodynamiques,» Document interne PSA, 2009.

Table of figures

Table of tables